CCN1 induces hepatic ductular reaction through integrin $\alpha_v\beta_5$–mediated activation of NF-κB

Ki-Hyun Kim,[1] Chih-Chiun Chen,[1] Gianfranco Alpini,[2,3,4] and Lester F. Lau[1]

[1]Department of Biochemistry and Molecular Genetics, University of Illinois at Chicago College of Medicine, Chicago, Illinois, USA. [2]Division of Research, Central Texas Veterans Health Care System, Temple, Texas, USA. [3]Scott & White Digestive Disease Research Center, Temple, Texas, USA. [4]Department of Internal Medicine, Texas A&M University Health Science Center, Temple, Texas, USA.

Liver cholestatic diseases, which stem from diverse etiologies, result in liver toxicity and fibrosis and may progress to cirrhosis and liver failure. We show that CCN1 (also known as CYR61), a matricellular protein that dampens and resolves liver fibrosis, also mediates cholangiocyte proliferation and ductular reaction, which are repair responses to cholestatic injury. In cholangiocytes, CCN1 activated NF-κB through integrin $\alpha_v\beta_5$/$\alpha_v\beta_3$, leading to *Jag1* expression, JAG1/NOTCH signaling, and cholangiocyte proliferation. CCN1 also induced *Jag1* expression in hepatic stellate cells, whereupon they interacted with hepatic progenitor cells to promote their differentiation into cholangiocytes. Administration of CCN1 protein or soluble JAG1 induced cholangiocyte proliferation in mice, which was blocked by inhibitors of NF-κB or NOTCH signaling. Knock-in mice expressing a CCN1 mutant that is unable to bind $\alpha_v\beta_5$/$\alpha_v\beta_3$ were impaired in ductular reaction, leading to massive hepatic necrosis and mortality after bile duct ligation (BDL), whereas treatment of these mice with soluble JAG1 rescued ductular reaction and reduced hepatic necrosis and mortality. Blockade of integrin $\alpha_v\beta_5$/$\alpha_v\beta_3$, NF-κB, or NOTCH signaling in WT mice also resulted in defective ductular reaction after BDL. These findings demonstrate that CCN1 induces cholangiocyte proliferation and ductular reaction and identify CCN1/$\alpha_v\beta_5$/NF-κB/JAG1 as a critical axis for biliary injury repair.

Introduction

The intrahepatic biliary tree functions to modify canalicular bile through secretory and reabsorptive processes in bile duct cholangiocytes. Disorders affecting the function and homeostasis of these biliary epithelial cells underlie cholangiopathies, diseases that account for 20% of adult liver transplantations (1, 2). Cholestatic diseases constitute a major group of cholangiopathies and may arise from diverse etiologies, including biliary obstruction from gallstones or tumor growth, inflammatory and autoimmune disorders including primary biliary cirrhosis and primary sclerosing cholangitis, and genetic deficiency in bile transport proteins (1, 2). Biliary obstruction leads to increases in bile acid accumulation in the liver and serum, liver toxicity, and ultimately fibrosis progressing to cirrhosis. A prominent response to biliary obstruction is ductular reaction, which occurs at the interphase of the portal and parenchymal compartments and is also observed in virtually all forms of human liver diseases (3). Ductular reaction is characterized by cholangiocyte proliferation, expansion of transit-amplifying cells or hepatic progenitor cells (HPCs), and differentiation of the bipotential HPCs into cholangiocytes and hepatocytes (3, 4). This process gives rise to an increased number of biliary ductules composed of "reactive cholangiocytes" that express inflammatory and chemotactic cytokines, leading to the recruitment of inflammatory and mesenchymal cells, thereby potentiating fibrosis (1, 5). Although a growing number of regulators that play important roles in ductular reaction have been identified, the cellular and molecular interactions that orchestrate and regulate ductular reaction during liver injury are still incompletely understood.

Studies have shown that cholangiocyte proliferation is under neuroendocrine control, and various hormones, neuropeptides, cytokines, and growth factors participate in its regulation (6, 7). By contrast, interaction of the Jagged1 (JAG1)-NOTCH2 ligand-receptor pair is critical for bile duct morphogenesis during embryonic development, and mutations in JAG1 or NOTCH2 cause Alagille syndrome, phenotypes of which include intrahepatic bile duct paucity (8–13). Recent studies have shown that JAG1/NOTCH signaling plays an important role in driving the differentiation of HPCs into cholangiocytes during liver injury and contributes to tissue repair (14, 15). In addition, changes in the extracellular matrix (ECM) have been observed in the ductular reaction niche, suggesting that dynamic turnover of the ECM is important for HPC expansion (16).

CCN1 (CYR61) is a matricellular protein of the CCN family, which includes 6 members in mammals that play diverse roles in embryonic development, inflammation, and injury repair (17). Like other ECM and matricellular proteins (18), CCN1 acts primarily through direct binding to distinct cell surface integrin receptors in a cell type–specific manner to regulate diverse cellular responses (19). Whereas *Ccn1*-null mice are embryonic lethal because of cardiovascular defects (20, 21), in adulthood CCN1 function is linked to the regulation of inflammation, wound healing, and tissue repair (19, 22). Indeed, CCN1 is highly expressed in chronic liver injuries induced by the hepatotoxin CCl_4 and cholestasis induced by bile duct ligation (BDL), and functions to dampen and resolve tissue fibrosis by triggering cellular senescence in activated myofibroblasts through integrin $\alpha_6\beta_1$, whereupon senescent

Conflict of interest: The authors have declared that no conflict of interest exists.
Submitted: October 3, 2014; **Accepted:** February 12, 2015.
Reference information: *J Clin Invest*. 2015;125(5):1886–1900. doi:10.1172/JCI79327.

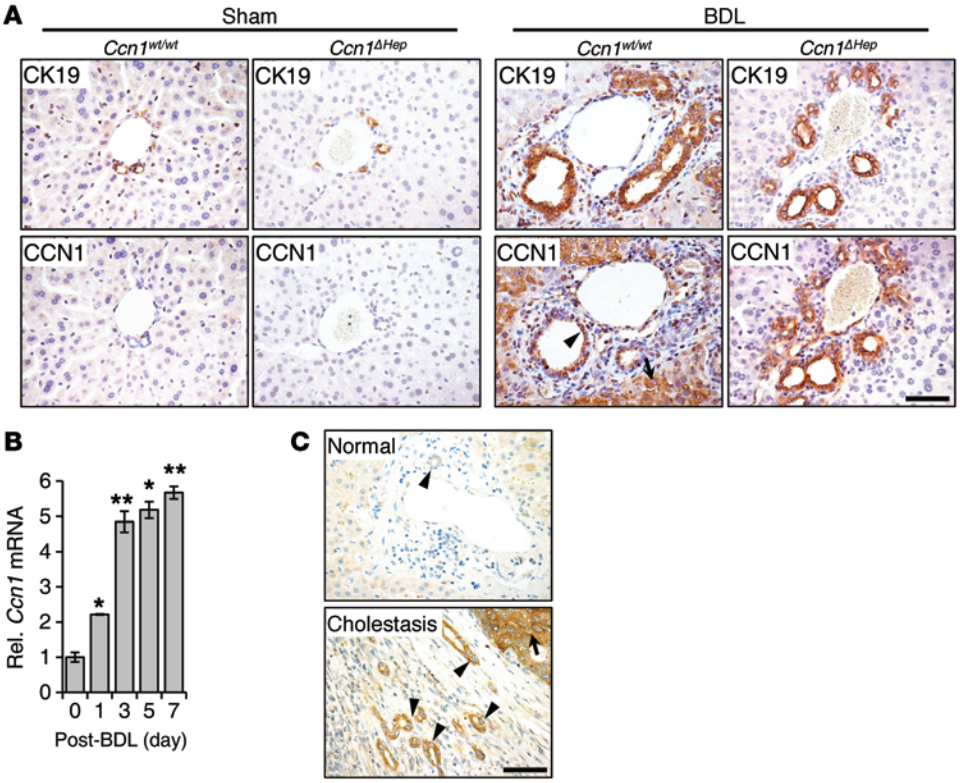

Figure 1. CCN1 is highly elevated in cholangiocytes in human and murine cholestatic livers. (**A**) Serial sections of liver from WT C57BL/6 and *Ccn1*$^{\Delta Hep}$ mice 7 days after sham operation or BDL were stained with antibodies against CK19 or CCN1 (brown), and counterstained with hematoxylin (blue). (**B**) *Ccn1* mRNA in WT mouse liver at indicated days after BDL was measured by qRT-PCR (n = 3). Data expressed as mean ± SD. *$P < 0.01$, **$P < 0.002$, Student's t test. (**C**) Representative images of immunohistochemical staining (brown) for CCN1 in normal and cholestatic human livers. Arrows point to hepatocytes, arrowheads to cholangiocytes. Scale bars: 50 μm.

myofibroblasts express an antifibrotic phenotype (23, 24). Given the reparative role of CCN1 in liver fibrosis, we have tested its potential function in regulating ductular reaction and biliary repair in cholestasis induced by BDL or chronic feeding of 3,5-diethoxycarbonyl-1,4-dihydrocollidine (DDC) (25).

Here we show that, unexpectedly, CCN1 is indispensable for ductular reaction and biliary repair. We reveal a novel pathway whereby CCN1 activates NF-κB in differentiated cholangiocytes through integrin $\alpha_v\beta_5/\alpha_v\beta_3$, leading to activation of *Jag1* expression and JAG1/NOTCH1 signaling to drive cholangiocyte proliferation. Furthermore, CCN1 also induces *Jag1* expression in hepatic stellate cells (HSCs) to promote cholangiocyte differentiation of HPCs. These findings uncover the essential role of the CCN1/$\alpha_v\beta_5$/NF-κB/JAG1 axis in bile duct regeneration and biliary injury repair.

Results

CCN1, acting through its $\alpha_v\beta_3/\alpha_v\beta_5$ binding site, is critical for survival after BDL. To evaluate the role of CCN1 in cholestatic diseases, we first examined its expression in mice subjected to BDL to induce cholestasis. Manifestations of murine ductular reaction in response to BDL include "typical" cholangiocyte proliferation (26), leading to increased cholangiocyte proliferation and intrahepatic bile duct mass within the portal areas (Figure 1A). In normal untreated WT mice, CCN1 was barely detectable by immunohistochemistry in hepatocytes and CK19-positive cholangiocytes, but increased to high levels in both cell types within 3–7 days after BDL (Figure 1A). When *Ccn1* was deleted specifically in hepatocytes in *Alb-Cre Ccn1*$^{fl/fl}$ (*Ccn1*$^{\Delta Hep}$) mice (24), CCN1 was increased in cholangiocytes but not hepatocytes after BDL as expected (Figure 1A). Interestingly, ductular reaction appeared normal in *Ccn1*$^{\Delta Hep}$ mice, indicating that hepatocyte-expressed CCN1 is dispensable for this process. Consistent with increased CCN1 protein, *Ccn1* mRNA levels rose steadily over 7 days after BDL (Figure 1B). Similarly, CCN1 was nearly undetectable in normal human liver; however, its expression increased in both hepatocytes and ductal cholangiocytes in cholestatic livers (Figure 1C), suggesting a role for CCN1 in response to cholestatic injury.

CCN1 plays diverse roles in various cell types through direct binding to distinct integrins (17, 19). Among the integrins that CCN1 binds are $\alpha_6\beta_1$, which is important for CCN1 functions in fibroblasts (27, 28), and $\alpha_v\beta_3$ and $\alpha_v\beta_5$, which are critical for its functions in vascular and epithelial cells (29, 30). We have previously identified the CCN1 binding sites for these integrins and created specific CCN1 mutations that prevent binding to these integrins (31, 32). Further, we have constructed an allelic series of knock-in mice in which the *Ccn1* genomic locus is replaced by either the *Ccn1*^{dm} allele, which encodes an $\alpha_6\beta_1$-binding-defective CCN1 (31), or the *Ccn1*^{D125A} allele, which encodes a single amino acid substitution (Asp-125 to Ala) that disrupts the non–arginylglycylaspartic acid–binding site of CCN1 for $\alpha_v\beta_3/\alpha_v\beta_5$ (32). Both *Ccn1*$^{dm/dm}$ and *Ccn1*$^{D125A/D125A}$ mice are viable and fertile and have histologically normal livers, indicating that CCN1 activities through these integrins are not required for liver development. The use of these knock-in mice allows us to dissect CCN1 functions through distinct integrins in vivo, circumvents the embryonic lethality of *Ccn1*-null mice (20, 21), and avoids potential limitations of cell type–specific deletions, as CCN1 may be secreted by multiple cell types in the tissue microenvironment.

To dissect the functions of CCN1 in cholestasis, we subjected *Ccn1*$^{wt/wt}$, *Ccn1*$^{\Delta Hep}$, *Ccn1*$^{dm/dm}$, and *Ccn1*$^{D125A/D125A}$ mice to BDL (33). Remarkably, 75% of *Ccn1*$^{D125A/D125A}$ mice perished within 7 days,

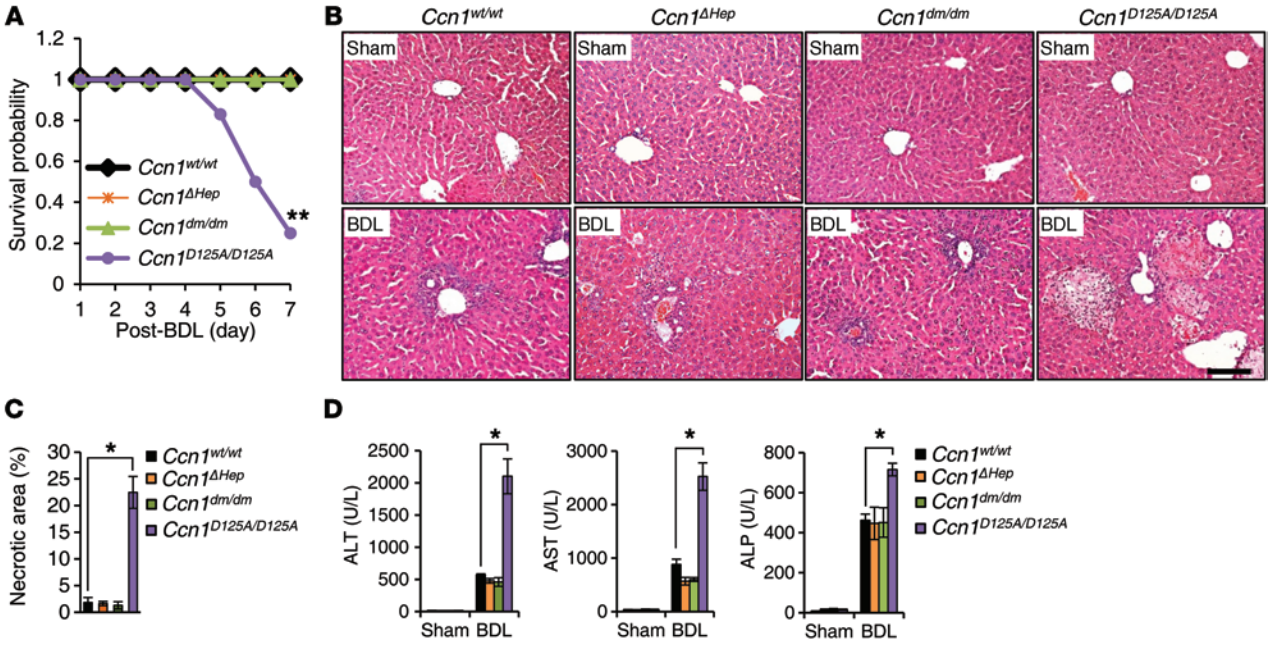

Figure 2. *Ccn1*$^{D125A/D125A}$ mice suffer massive hepatic necrosis and mortality after BDL. *Ccn1*$^{wt/wt}$, *Ccn1*$^{\Delta Hep}$, *Ccn1*$^{dm/dm}$, and *Ccn1*$^{D125A/D125A}$ mice were subjected to sham operation or BDL and sacrificed 7 days later. (**A**) Survival curve after BDL (n = 12 each). **P < 0.001, log-rank test. (**B**) Liver sections were stained with H&E. (**C**) Percentages of necrotic area were determined by ImageJ software (n = 6 each). *P < 0.02, Student's t test. (**D**) Serum levels of alanine aminotransferase (ALT), aspartate aminotransferase (AST), and alkaline phosphatase (ALP) were analyzed (n = 6 each). *P < 0.02, Student's t test. Data represent means ± SD of the results determined in triplicate experiments. Scale bar: 100 μm.

whereas 100% of *Ccn1*$^{wt/wt}$, *Ccn1*$^{\Delta Hep}$, and *Ccn1*$^{dm/dm}$ mice survived during this period (Figure 2A). All 4 genotypes exhibited normal liver histology before injury, and *Ccn1*$^{wt/wt}$, *Ccn1*$^{\Delta Hep}$, and *Ccn1*$^{dm/dm}$ mice experienced submassive hepatic necrosis after BDL as expected (34). However, *Ccn1*$^{D125A/D125A}$ mice showed approximately 12-fold more necrotic areas in their livers after BDL, covering approximately 20% of the liver parenchyma (Figure 2, B and C). *Ccn1*$^{D125A/D125A}$ mice displayed greatly elevated levels of serum alanine aminotransferase and aspartate aminotransferase after BDL, indicating more severe hepatocyte damage, and increased serum alkaline phosphatase, indicating enhanced cholestatic damage (Figure 2D). Hepatic necrosis as a result of cholestasis may be due to cytotoxicity from accumulating bile acids (35). However, we found that primary hepatocytes isolated from *Ccn1*$^{wt/wt}$ or *Ccn1*$^{D125A/D125A}$ mice were equally susceptible to cell death induced by the bile acid glycochenodeoxycholic acid (GCDCA) or glycocholate (GCA; Supplemental Figure 1; supplemental material available online with this article; doi:10.1172/JCI79327DS1). Moreover, the total amounts of bile acids in the liver and serum were the same in *Ccn1*$^{wt/wt}$ and *Ccn1*$^{D125A/D125A}$ mice, indicating that there was no difference in bile acid production (Supplemental Figure 1). Thus, the massive hepatic necrosis and lethality of *Ccn1*$^{D125A/D125A}$ mice in response to BDL may be due to defects in the liver injury response rather than differential sensitivity of hepatocytes to bile acids or increase in bile acid synthesis. These phenotypes are specific to *Ccn1*$^{D125A/D125A}$ mice, indicating that CCN1 plays crucial roles in response to BDL through its $\alpha_v\beta_3/\alpha_v\beta_5$ binding site.

CCN1-$\alpha_v\beta_5$ interaction is required for cholangiocyte proliferation in cholestasis. Ductular reaction induced by cholestatic biliary damage includes proliferation of cholangiocytes, resulting in bile duct expansion and proliferation (3). *Ccn1*$^{wt/wt}$, *Ccn1*$^{\Delta Hep}$, and *Ccn1*$^{dm/dm}$ mice all showed an increase in the number of CK19-positive intrahepatic bile ducts characteristic of BDL injury, whereas *Ccn1*$^{D125A/D125A}$ mice were severely impaired in this response, leading to a relative paucity of intrahepatic bile ducts after BDL (Figure 3A). Staining for the proliferation marker proliferating cell nuclear antigen (PCNA) showed that many cholangiocytes were proliferating in *Ccn1*$^{wt/wt}$, *Ccn1*$^{\Delta Hep}$, and *Ccn1*$^{dm/dm}$ mice, but not in *Ccn1*$^{D125A/D125A}$ mice (Figure 3B). To assess whether impaired ductular reaction in *Ccn1*$^{D125A/D125A}$ mice is unique to BDL-induced cholestasis, we used another well-established model of biliary damage induced by chronic DDC feeding, which triggers obstructive cholestasis from precipitation of protoporphyrins within the intrahepatic bile ducts (2, 36). As expected, *Ccn1*$^{wt/wt}$ mice exhibited an "atypical" cholangiocyte proliferation response after 6 weeks of DDC diet (25), with proliferation of intrahepatic bile ducts sprouting into both the periportal and parenchymal regions (Figure 3C). By contrast, *Ccn1*$^{D125A/D125A}$ mice showed significantly reduced biliary proliferation compared with *Ccn1*$^{wt/wt}$ mice as evidenced by CK19 and PCNA staining, indicating a defect in ductular reaction (Figure 3C). Proliferation of small ductules in the DDC diet model is thought to involve significant participation of HPCs (37), suggesting that expansion of the progenitor compartment is also impaired in *Ccn1*$^{D125A/D125A}$ mice.

Results above indicate that CCN1 is critical for cholangiocyte proliferation and ductular reaction induced by BDL and DDC diet, whereas hepatocyte proliferation was unaffected by the *Ccn1* mutation (Supplemental Figure 2). Since ductular reaction is a complex process that includes cholangiocyte proliferation and differentiation of HPCs into cholangiocytes (16), we sought to establish the mitogenic effect of CCN1 on cholangiocytes in vivo, inde-

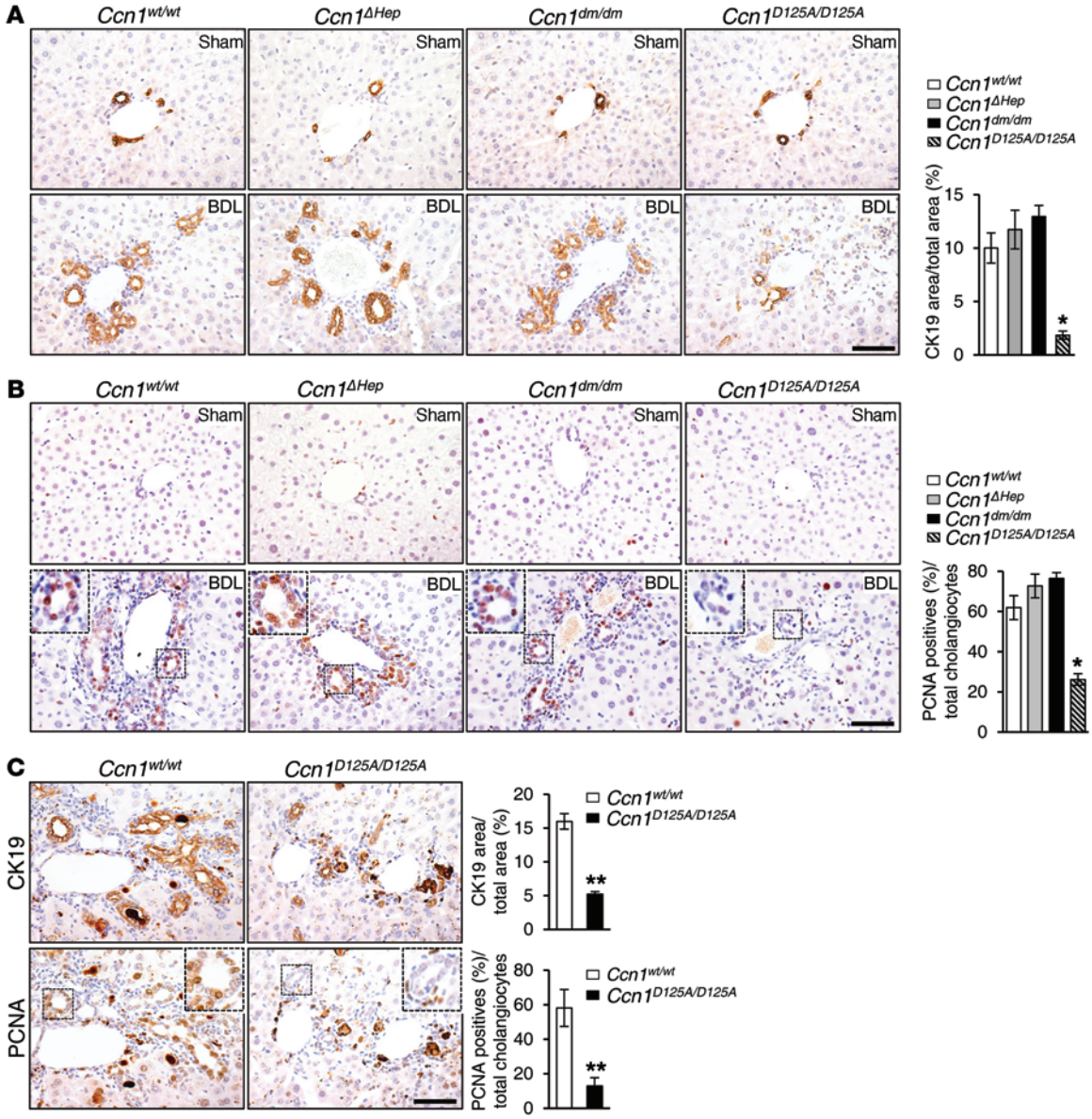

Figure 3. Blunted biliary ductal reaction in *Ccn1*$^{D125A/D125A}$ mice following BDL or DDC diet. (**A**) Liver sections from either sham- or BDL-operated *Ccn1*$^{wt/wt}$, *Ccn1*$^{\Delta Hep}$, *Ccn1*$^{dm/dm}$, and *Ccn1*$^{D125A/D125A}$ mice were stained with anti-CK19 antibodies, and the average percentage of CK19-positive area in each genotype was quantified and expressed as mean ± SD. (n = 6 per group.) *P < 0.001, Student's t test. (**B**) Adjacent tissue sections from above were stained with anti-PCNA antibodies, and the percentage of PCNA-positive cholangiocytes for each genotype was quantified and expressed as mean ± SD. (n = 6 per group.) *P < 0.001, Student's t test. (**C**) Serial sections of liver tissue from mice fed DDC diet for 6 weeks were immunostained for CK19 or PCNA (n = 6). **P < 0.0001, Student's t test. Note that some of the brown-staining areas were due to protoporphyrin crystals resulting from the DDC diet. Scale bars: 50 μm.

pendent of induced biliary injury. The peribiliary vascular plexus (PBP) that supplies blood to the bile ducts is an anastomotic network derived from the hepatic arterial branches and flows into the hepatic sinusoids. Capillaries of the PBP are highly fenestrated, facilitating the exchange of molecules between the bile duct and the PBP (38). Thus, when injected into WT mice via retro-orbital delivery, purified CCN1 protein is rapidly and extensively localized in the liver (Supplemental Figure 3). Remarkably, injection of CCN1 alone was sufficient to stimulate cholangiocyte proliferation within 2–4 days as judged by PCNA staining of CK19-positive intrahepatic bile ducts (Figure 4A), indicating that CCN1 is mitogenic for differentiated bile duct cholangiocytes.

Cholangiocytes in the intrahepatic biliary tree are morphologically and functionally heterogeneous and are composed of large and small cholangiocytes, which line ducts greater than 15 μm and ductules less than 15 μm in diameter, respectively (39). Since proliferation after BDL occurs specifically in large cholangiocytes (40), we examined CCN1 function in the proliferation of large mouse cholangiocyte cultures (LMCCs) (41). These cells express a level of CCN1 that was easily detectable by immunoblotting; downregulation of endogenous CCN1 by *siCcn1* strongly inhibited proliferation as evaluated by cell number counts and BrdU incorporation (Figure 4, B and C), without affecting apoptosis or senescence (Supplemental Figure 4). Addition of purified WT CCN1

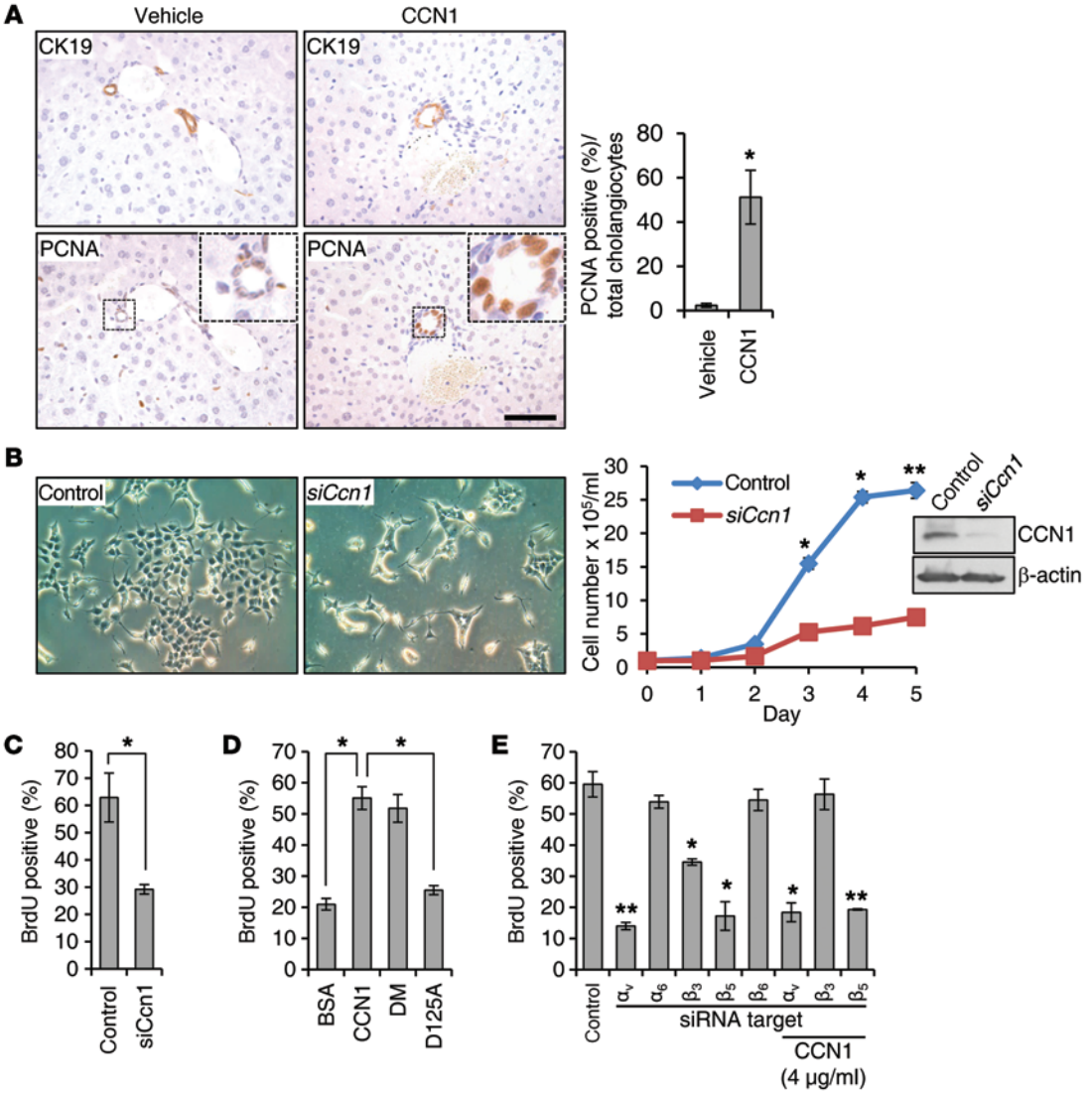

Figure 4. CCN1 promotes cholangiocyte proliferation through integrins $\alpha_v\beta_5$ and $\alpha_v\beta_3$. (**A**) Serial liver sections from normal WT mice injected with CCN1 (1 mg/kg) or vehicle daily via retro-orbital delivery were immunostained for CK19 or PCNA, and percentages of PCNA-positive cholangiocytes were quantified and expressed as mean ± SD. (n = 6 per group.) *P < 0.01, Student's t test. (**B**) LMCCs were transfected with either CCN1-targeting siRNA or nontargeting control RNA. Micrographs show cells 3 days after siRNA transfection, and growth curve shows effects of *siCcn1*. Immunoblotting shows CCN1 knockdown by *siCcn1*. *P < 0.01, **P < 0.003, Student's t test. (**C**) BrdU incorporation assay carried out on LMCCs 2 days after transfection of siRNA; percentages of BrdU-positive cells were counted in 5 high-power fields. *P < 0.01, Student's t test. (**D**) Cells were treated overnight with purified recombinant WT CCN1, CCN1-DM, CCN1-D125A, or BSA (4 μg/ml each), and percentages of BrdU-positive cells were counted as above. *P < 0.01, Student's t test. (**E**) BrdU incorporation assay was conducted in LMCCs transfected with control RNA or siRNAs targeting integrins α_v, α_6, β_3, β_5, and β_6. Where indicated, CCN1 (4 μg/ml) was added 1 day after siRNA treatment. Knockdown of integrins was confirmed by qRT-PCR (Supplemental Figure 6). *P < 0.01, **P < 0.003, Student's t test. Data in **C**–**E** expressed as mean ± SD of triplicate determinations. Scale bar: 50 μm.

or CCN1-DM mutant protein ($\alpha_6\beta_1$-binding-defective) to LMCCs stimulated DNA synthesis, but the CCN1-D125A mutant protein ($\alpha_v\beta_3/\alpha_v\beta_5$-binding-defective) was unable to do so (refs. 31, 32, and Figure 4D). Further increased expression of *Ccn1* via adenovirus transduction also enhanced proliferation (Supplemental Figure 5). These results indicated that endogenously expressed *Ccn1* is required for the proliferation of large cholangiocytes, and exogenously added CCN1 further promotes cholangiocyte proliferation.

Since the inability of CCN1-D125A to stimulate cholangiocyte proliferation indicates that CCN1 functions through its $\alpha_v\beta_3/\alpha_v\beta_5$ binding site, we used RNAi knockdown of specific integrin subunits to pinpoint the critical receptors. Knockdown of integrins was accomplished with efficiency (Supplemental Figure 6) and revealed that targeting integrin α_6 had no effect, whereas knockdown of α_v dramatically reduced proliferation (Figure 4E). Among α_v integrin heterodimers, CCN1 is known to bind $\alpha_v\beta_3$ and $\alpha_v\beta_5$, and $\alpha_v\beta_6$ has been implicated in cholangiocyte function (19, 42). Knockdown of β_5 severely inhibited cholangiocyte proliferation, whereas knockdown of β_3 was partially inhibitory and knockdown of β_6 had no effect (Figure 4E), indicating that CCN1 induces cholangiocyte proliferation primarily through $\alpha_v\beta_5$, with $\alpha_v\beta_3$ playing an auxiliary role. Consistent with this interpretation, exogenously added CCN1

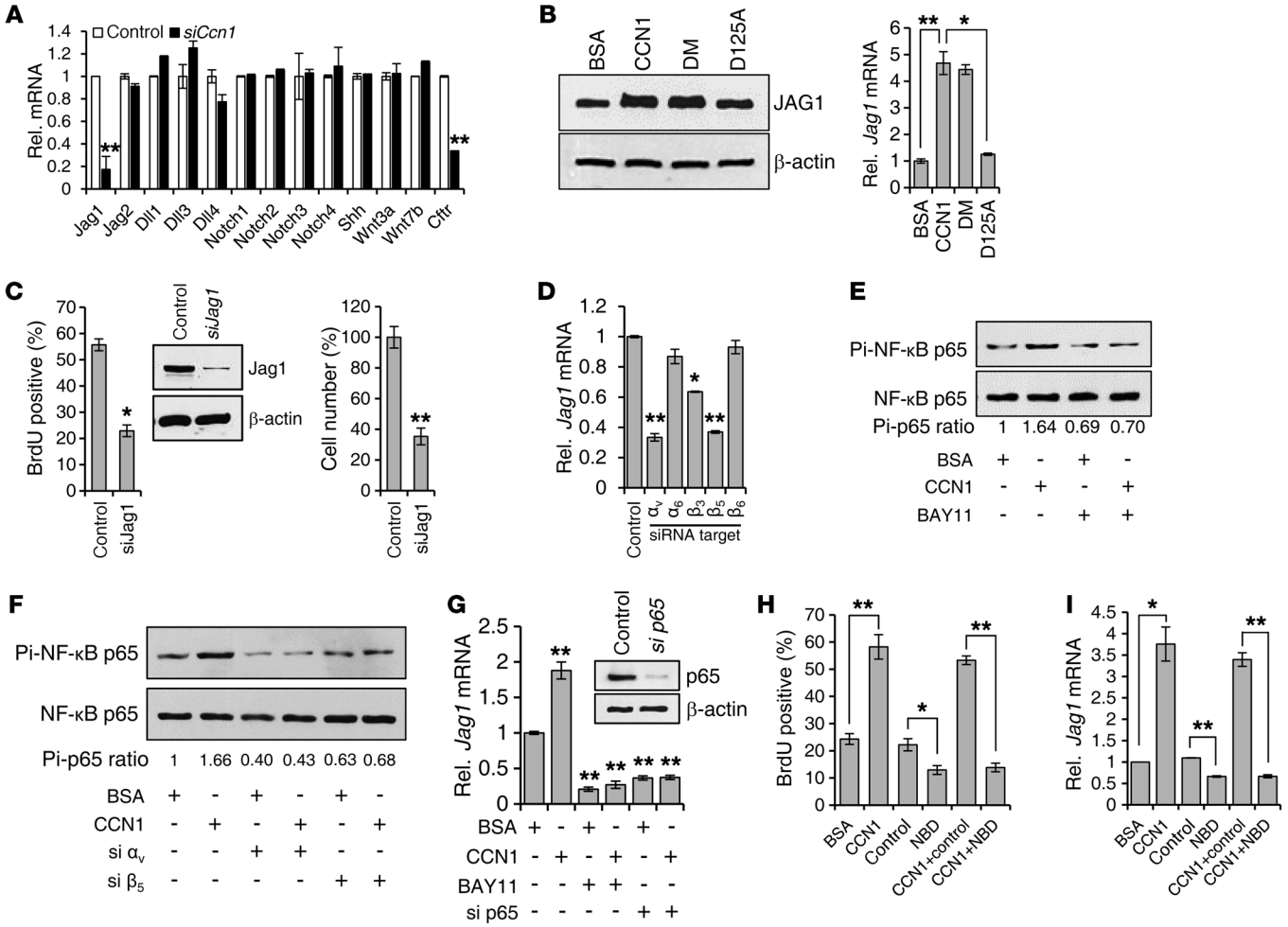

Figure 5. CCN1 promotes cholangiocyte proliferation through NF-κB–mediated *Jag1* expression. (**A**) Expression of indicated genes was assessed by qRT-PCR in LMCCs transfected with *siCcn1* or control siRNA. $^{**}P < 0.004$, Student's *t* test. (**B**) JAG1 protein was detected by immunoblotting in lysates of LMCCs incubated with WT CCN1, CCN1-DM, CCN1-D125A, or BSA (4 μg/ml each) for 2 days, and *Jag1* mRNA was quantified by qRT-PCR. $^{*}P < 0.02$, $^{**}P < 0.004$, Student's *t* test. (**C**) BrdU incorporation and total cell numbers were assessed in cholangiocytes 2 days after transfection with *siJag1* or control siRNA. Knockdown of JAG1 was confirmed by immunoblotting. $^{*}P < 0.02$, $^{**}P < 0.004$, Student's *t* test. (**D**) *Jag1* mRNA was measured by qRT-PCR in cells treated with siRNAs targeting indicated integrins. $^{*}P < 0.02$, $^{**}P < 0.004$, Student's *t* test. (**E**) Phosphorylation of NF-κB p65 was detected by immunoblotting in cholangiocytes incubated with CCN1 for 3 hours with or without pretreatment (30 minutes) with BAY11-7082 (5 μM). Levels of phosphorylated p65 were normalized to total p65. Pi, phosphorylated. (**F**) LMCCs were treated with siRNA targeting indicated integrins before CCN1 treatment and assayed for phosphorylation of NF-κB p65 by immunoblotting. (**G**) *Jag1* mRNA was measured by qRT-PCR in LMCCs treated with CCN1 for 3 hours, with or without preincubation with BAY11-7082, or in cells transfected with siRNA targeting NF-κB p65. Knockdown of p65 was confirmed by immunoblotting. $^{**}P < 0.004$, Student's *t* test. (**H**) BrdU incorporation was assessed in LMCCs treated with BSA (4 μg/ml), CCN1 (4 μg/ml), NBD (25 μM), or control peptide (25 μM). $^{*}P < 0.02$, $^{**}P < 0.004$, Student's *t* test. (**I**) *Jag1* mRNA expression was analyzed with cells treated as in **H**. $^{*}P < 0.02$, $^{**}P < 0.004$, Student's *t* test. All data are expressed as mean ± SD of triplicate determinations.

protein was unable to rescue the growth-inhibitory effects of α_v or β_5 knockdown, as they play essential roles (Figure 4E). However, addition of CCN1 mitigated the inhibitory effects of β_3 knockdown, most likely because exogenously added CCN1 compensated for the loss of $\alpha_v\beta_3$ by increased engagement of $\alpha_v\beta_5$ (Figure 4E).

CCN1 induces cholangiocyte proliferation through $\alpha_v\beta_5$-dependent activation of NF-κB. To elucidate the mechanisms of CCN1 action, we first examined whether CCN1 regulates the expression of genes implicated in cholangiocyte differentiation and proliferation. Strikingly, treatment of cells with *siCcn1* resulted in significant downregulation of *Jag1*, whereas no effect was observed in the expression of *Shh*, *Wnt3a*, and *Wnt7b* (Figure 5A). In mammals, JAG1, JAG2, DLL1, DLL3, and DLL4 constitute the 5 canonical ligands of NOTCH receptors, which include NOTCH1, NOTCH2, NOTCH3, and NOTCH4 (43). However, expression of *Notch1–Notch4*, *Jag2*, *Dll1*, *Dll3*, and *Dll4* was not significantly affected by *siCcn1* (Figure 5A). The cystic fibrosis transmembrane conductance regulator (*CFTR*) gene was also downregulated by *Ccn1* knockdown, indicating that CCN1 is important for cholangiocyte function (Figure 5A). Moreover, purified CCN1 or CCN1-DM proteins elevated *Jag1* mRNA and protein levels in cholangiocytes, whereas CCN1-D125A was unable to do so, consistent with CCN1 function through its $\alpha_v\beta_3/\alpha_v\beta_5$ binding site (Figure 5B). Knockdown of *Jag1* by siRNA in cholangiocytes inhibited cell proliferation as measured by BrdU incorporation and cell number (Figure 5C), confirming that *Jag1* plays a critical role in cholangiocyte proliferation.

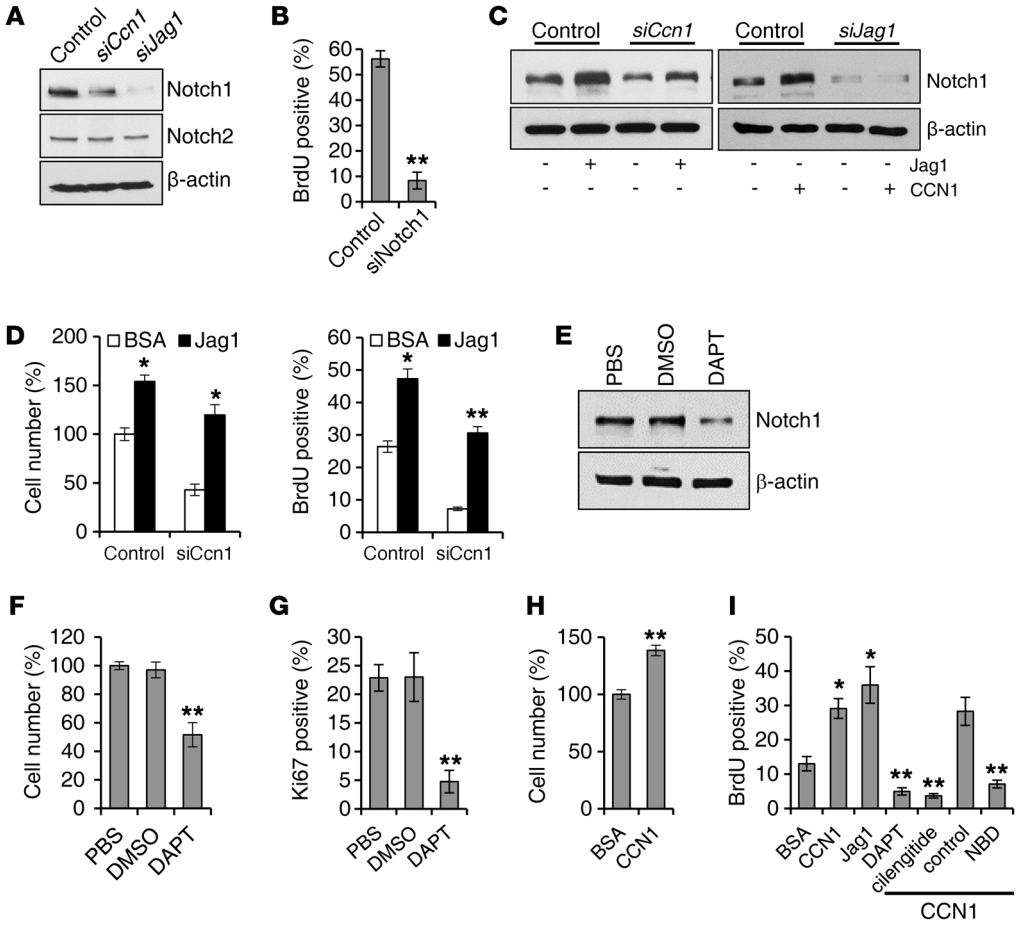

Figure 6. CCN1 promotes cholangiocyte proliferation through JAG1/NOTCH1 pathway. (**A**) Protein lysates of LMCCs transfected with siRNAs targeting *Ccn1* or *Jag1* were analyzed for NICD of NOTCH1 and NOTCH2 by immunoblotting. (**B**) Proliferation of cholangiocytes transfected with *siNotch1* was assessed by BrdU incorporation. $^{**}P < 0.01$, Student's *t* test. (**C**) NOTCH 1 NICD was detected by immunoblotting in cells treated with *siCcn1, siJag1,* or a nontargeting control and incubated with or without soluble JAG1 (2 μg/ml), CCN1 (4 μg/ml), or BSA for 2 days. (**D**) Proliferation of cells treated with *siCcn1* or control siRNA and incubated with or without soluble JAG1 (2 μg/ml) was evaluated by cell numbers and BrdU incorporation. $^{*}P < 0.04$, $^{**}P < 0.01$, Student's *t* test. (**E**) NOTCH1 NICD was detected by immunoblotting in cholangiocytes incubated with DAPT (10 μM) or vehicle (DMSO) for 24 hours. (**F** and **G**) Proliferation of cells was assessed by counting of cell numbers (**F**) and immunohistochemical detection of Ki67-positive cells (**G**). Percentages of Ki67-positive cells relative to total number of cells were counted in 5 randomly chosen high-power fields. $^{**}P < 0.01$, Student's *t* test. (**H**) Freshly isolated primary cholangiocytes (98.5% ± 0.4% IgG2a-positive) were cultured with BSA or CCN1 (4 μg/ml) for 2 days, and proliferation was assessed by cell numbers. $^{**}P < 0.01$, Student's *t* test. (**I**) BrdU incorporation was quantified in freshly isolated primary cholangiocytes treated with BSA (4 μg/ml), CCN1 (4 μg/ml), soluble JAG1 (2 μg/ml), DAPT (10 μM), cilengitide (1 μM), NBD (25 μM), or control peptide (25 μM). Where indicated, CCN1 (4 μg/ml) was added with other inhibitors. $^{*}P < 0.04$, $^{**}P < 0.01$, Student's *t* test. All data are expressed as mean ± SD of triplicate determinations.

Consistent with the integrin requirement for CCN1-induced cholangiocyte proliferation (Figure 4E), siRNA knockdown of integrin α_v and β_5 significantly inhibited *Jag1* expression but knockdown of α_6 or β_6 had no effect, whereas knockdown of β_3 was partially inhibitory (Figure 5D and Supplemental Figure 6). Since *Jag1* can be regulated by multiple pathways including NF-κB signaling and CCN1 is known to activate NF-κB (22, 44), we hypothesized that CCN1 may activate *Jag1* through NF-κB. CCN1 stimulated the activation of NF-κB as judged by p65 NF-κB phosphorylation, which was blocked by the IKK inhibitor BAY11-7082, showing that CCN1 activates NF-κB in cholangiocytes (Figure 5E). CCN1-dependent stimulation of p65 phosphorylation was inhibited by siRNA knockdown of integrin α_v and β_5, demonstrating that CCN1 activates NF-κB through $\alpha_v\beta_5$ (Figure 5F). Moreover, siRNA knockdown of p65, or treatment with BAY11-7082, blocked CCN1 upregulation of *Jag1* expression (Figure 5G). To demonstrate further that the proliferative effects of CCN1 on cholangiocytes are mediated through NF-κB, we have also used the NEMO-binding domain (NBD) peptide to inhibit NF-κB activation (45). The presence of the NBD peptide, but not the control peptide, inhibited CCN1-stimulated cholangiocyte DNA synthesis (Figure 5H). Likewise, CCN1-induced *Jag1* expression was blocked by the presence of the NBD peptide, but not the control peptide (Figure 5I). Consistently, CCN1 induces the expression of genes important for cell proliferation, including *Ccnd1* and *IL6*, through activation of NF-κB (Supplemental Figure 7). Together, these results show that CCN1 activates NF-κB through integrin $\alpha_v\beta_5$, leading to expression of *Jag1* and proliferation of cholangiocytes.

NF-κB–activated Jag1/Notch signaling mediates CCN1-induced cholangiocyte proliferation in vitro and in vivo. Engagement of the integral membrane protein JAG1 with its membrane receptor

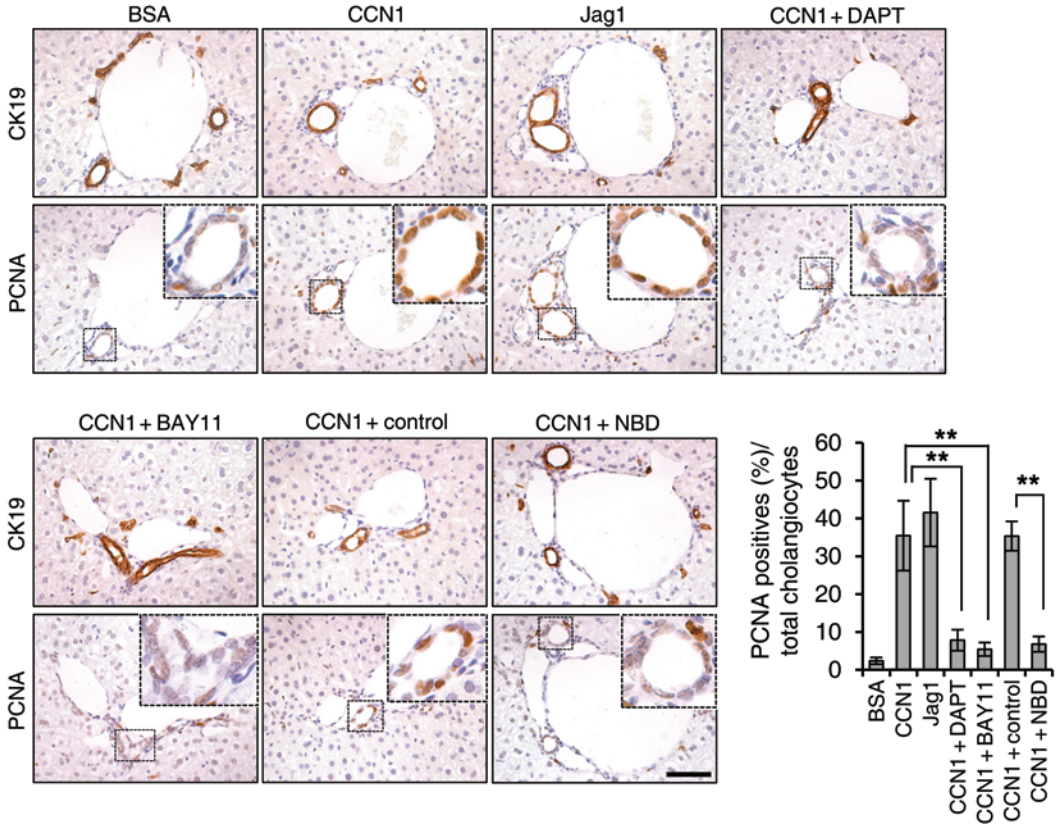

Figure 7. CCN1 induces cholangiocyte proliferation through NF-κB and NOTCH signaling in vivo. Adjacent liver sections of WT mice injected with CCN1 (1 mg/kg), soluble JAG1 (0.5 mg/kg), or BSA (1 mg/kg) by retro-orbital delivery were immunostained for CK19 or PCNA, and percentages of PCNA-positive cholangiocytes were quantified and expressed as mean ± SD. (n = 6 per group.) $^{**}P < 0.01$, Student's t test. Where indicated, DAPT (10 mg/kg), BAY11-7082 (5 mg/kg), NBD (1 mg/kg), or control peptide (1 mg/kg) was coinjected. Scale bar: 50 μm.

NOTCH leads to processing of NOTCH by γ-secretase, releasing the NOTCH intracellular domain (NICD) that translocates into the nucleus, where it interacts with RBPJk to regulate transcription of downstream target genes including *Hes1* (43). Addition of CCN1 to cholangiocytes enhanced expression of the NOTCH target genes *Hes1* and *Hnf1b*, whereas *siCcn1* inhibited their expression, suggesting that CCN1 activates NOTCH signaling (Supplemental Figure 8, A and B). Knockdown of either *Ccn1* or *Jag1* by siRNA substantially reduced the amount of NOTCH1 NICD released, but had no effect on NOTCH2 NICD, indicating that NOTCH1 is the principal JAG 1 receptor in this context (Figure 6A). Consistent with this interpretation, siRNA knockdown of NOTCH1 abrogated BrdU incorporation in LMCCs (Figure 6B), indicating that JAG1/NOTCH1 signaling is required for cholangiocyte proliferation. Furthermore, the addition of either CCN1 or a soluble JAG1 that can activate NOTCH signaling (46) was able to stimulate NICD release (Figure 6C). However, whereas soluble JAG1 rescued the inhibitory effects of *Ccn1* knockdown on NICD release, CCN1 addition was unable to reverse the inhibitory effects of JAG1 knockdown, consistent with JAG1 acting downstream of CCN1 (Figure 6C).

Whereas previous studies have shown that JAG1 is required for differentiation of cholangiocytes from HPCs, its role in proliferation of differentiated cholangiocytes is unknown (15). Addition of the NOTCH-activating soluble JAG1 alone was sufficient to increase cholangiocyte proliferation as judged by cell number and BrdU incorporation, indicating that JAG1 can stimulate cholangiocyte proliferation (Figure 6D). Moreover, soluble JAG1 rescued the inhibitory effect of *siCcn1* on cell proliferation, suggesting that JAG1 functions downstream of CCN1 (Figure 6D). Thus, CCN1 stimulation of cholangiocyte proliferation can be supplanted by exogenously added JAG1, indicating that CCN1 acts by inducing JAG1.

Since NOTCH signaling is mediated through NICD release, the γ-secretase inhibitor *N*-[*N*-(3,5-difluorophenacetyl)-L-alanyl]-S-phenylglycine *t*-butyl ester (DAPT) has been widely used to block NOTCH signaling. Consistent with CCN1 inducing cholangiocyte proliferation through NOTCH signaling, DAPT blocked the release of the NOTCH1 NICD and effectively inhibited cholangiocyte proliferation in vitro, causing a significant decrease in total cell number and percentage of Ki67-positive cells (Figure 6, E–G).

Since the CCN1-induced cholangiocyte proliferation pathway above was delineated in LMCCs, we sought to assess whether this pathway functions in primary cholangiocytes. Thus, we isolated primary cholangiocytes (98.5% IgG2a-positive), and found that CCN1 promotes their proliferation by cell number counts (Figure 6H). Furthermore, CCN1 and JAG1 both enhanced DNA synthesis as judged by BrdU labeling, and CCN1-stimulated DNA synthesis was blocked by an inhibitor of NOTCH signaling (DAPT) or NF-κB activation (NBD peptide), and abrogated by cilengitide (47), a cyclic pentapeptide that blocks $\alpha_v\beta_3$ and $\alpha_v\beta_5$ integrins (Figure 6I).

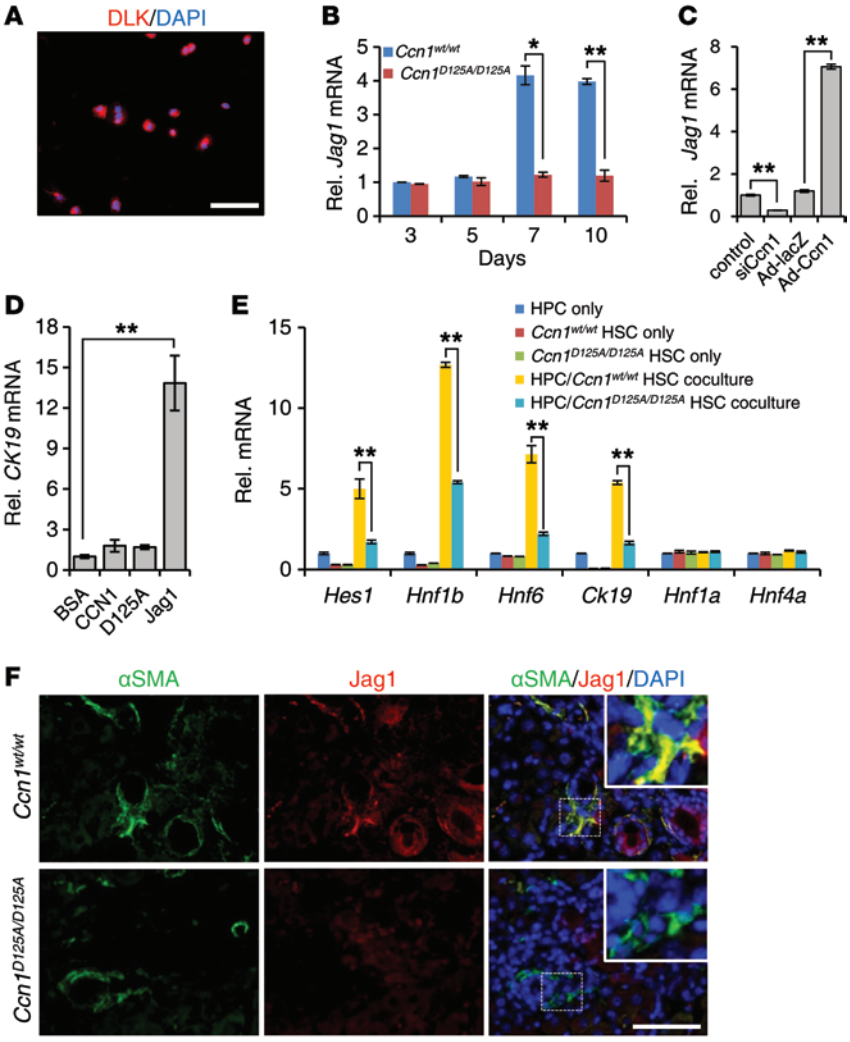

Figure 8. *Ccn1*$^{D125A/D125A}$ HSCs are impaired in *Jag1* expression and promotion of HPC differentiation to cholangiocytes. (**A**) HPCs isolated from normal mouse livers were cultured overnight and stained with anti-DLK1 antibodies and counterstained with DAPI; 93.8% ± 1.27% of isolated cells stained positive for DLK1. (**B**) *Jag1* expression was analyzed by qRT-PCR in HSCs at indicated days in culture after isolation from *Ccn1*$^{wt/wt}$ and *Ccn1*$^{D125A/D125A}$ mice. Data expressed as mean ± SD of triplicate determinations. $^{*}P < 0.02$, $^{**}P < 0.005$, Student's *t* test. (**C**) HSCs from *Ccn1*$^{wt/wt}$ mice were transfected with *siCcn1* or control RNA, or transduced with *Ad-Ccn1* virus or *Ad-LacZ* virus as a control. *Jag1* mRNA levels were analyzed by qRT-PCR after 3 days. Data expressed as mean ± SD of triplicate determinations. $^{**}P < 0.005$, Student's *t* test. (**D**) Expression of CK19 was measured by qRT-PCR in primary HPCs treated with BSA, WT CCN1, CCN1-D125A, or soluble JAG1 (4 μg/ml each). Data expressed as mean ± SD of triplicate determinations. $^{**}P < 0.005$, Student's *t* test. (**E**) Expression of cholangiocyte and hepatocyte marker genes was detected by qRT-PCR in 10-day cocultures of primary WT HPCs and HSCs isolated from *Ccn1*$^{wt/wt}$ and *Ccn1*$^{D125A/D125A}$ mice. Data expressed as mean ± SD of triplicate determinations. $^{**}P < 0.005$, Student's *t* test. (**F**) Liver sections from mice fed DDC diet for 6 weeks were double immunostained for α-smooth muscle actin (αSMA, green) and JAG1 (red) and counterstained with DAPI ($n = 6$). Scale bars: 50 μm.

These results confirmed that CCN1 induces proliferation through the $\alpha_v\beta_5$/NF-κB/JAG1-NOTCH axis in primary cholangiocytes.

To test whether the above signaling pathways for CCN1-induced cholangiocyte proliferation function in vivo, we injected either BSA or CCN1 into mice via retro-orbital delivery. As expected, CCN1 induced cholangiocyte proliferation (Figure 7). Consistent with CCN1 acting through induction of *Jag1*, injection of soluble JAG1 alone was also able to induce cholangiocyte proliferation (Figure 7). Injection of CCN1 together with DAPT inhibited the effect of CCN1, showing that CCN1 induces cholangiocyte proliferation through NOTCH signaling. Furthermore, coinjection of CCN1 with BAY11-7082 or NBD peptide effectively blocked the mitogenic effect of CCN1, whereas a control peptide had no effect. These results show that CCN1 stimulates cholangiocyte proliferation through NF-κB–induced JAG1/NOTCH signaling in vivo.

CCN1-regulated Jag1 expression in hepatic fibroblasts promotes progenitor cell differentiation into cholangiocytes. Upon liver injury, the bipotential HPCs can differentiate into hepatocytes and cholangiocytes and contribute to the liver regenerative response (14). It was recently shown that *Jag1* expressed in hepatic fibroblasts activates NOTCH in HPCs through juxtacrine signaling, thereby driving cholangiocyte differentiation during cholestatic injury (14). The deficiency of ductular reaction in *Ccn1*$^{D125A/D125A}$ mice, particularly following DDC diet (Figure 3C), suggests that CCN1 plays a role in the progenitor niche during ductular reaction. Thus, we postulated that CCN1 may regulate *Jag1* expression in hepatic fibroblasts to promote HPCs' differentiation into cholangiocytes, thereby contributing to cholestatic injury repair. To test this hypothesis, we isolated HPCs (Figure 8A) and primary HSCs, which are vitamin A storage cells that differentiate into myofibroblastic cells upon activation and are major precursor cells of hepatic fibroblasts (48). We found that *Jag1* expression increased in HSCs from *Ccn1*$^{wt/wt}$ mice over 7–10 days in culture, but not in HSCs from *Ccn1*$^{D125A/D125A}$ mice (Figure 8B). Consistent with regulation by CCN1, *Jag1* expression in HSCs was inhibited by siRNA knockdown of *Ccn1*, and greatly increased by adenoviral expression of *Ccn1* (Figure 8C). To test whether CCN1 protein may by itself have a direct effect on HPC differentiation, freshly isolated primary HPCs were treated with CCN1-WT, CCN1-D125A, or soluble JAG1 (Figure 8D). Soluble JAG1, but not WT or mutant CCN1 protein, was able to stimulate CK19 expression in these cells, indicating cholangiocyte differentiation. To assess whether CCN1-regulated *Jag1* expression in HSCs may act in juxtacrine to promote cholangiocyte differentiation in HPCs, we cocul-

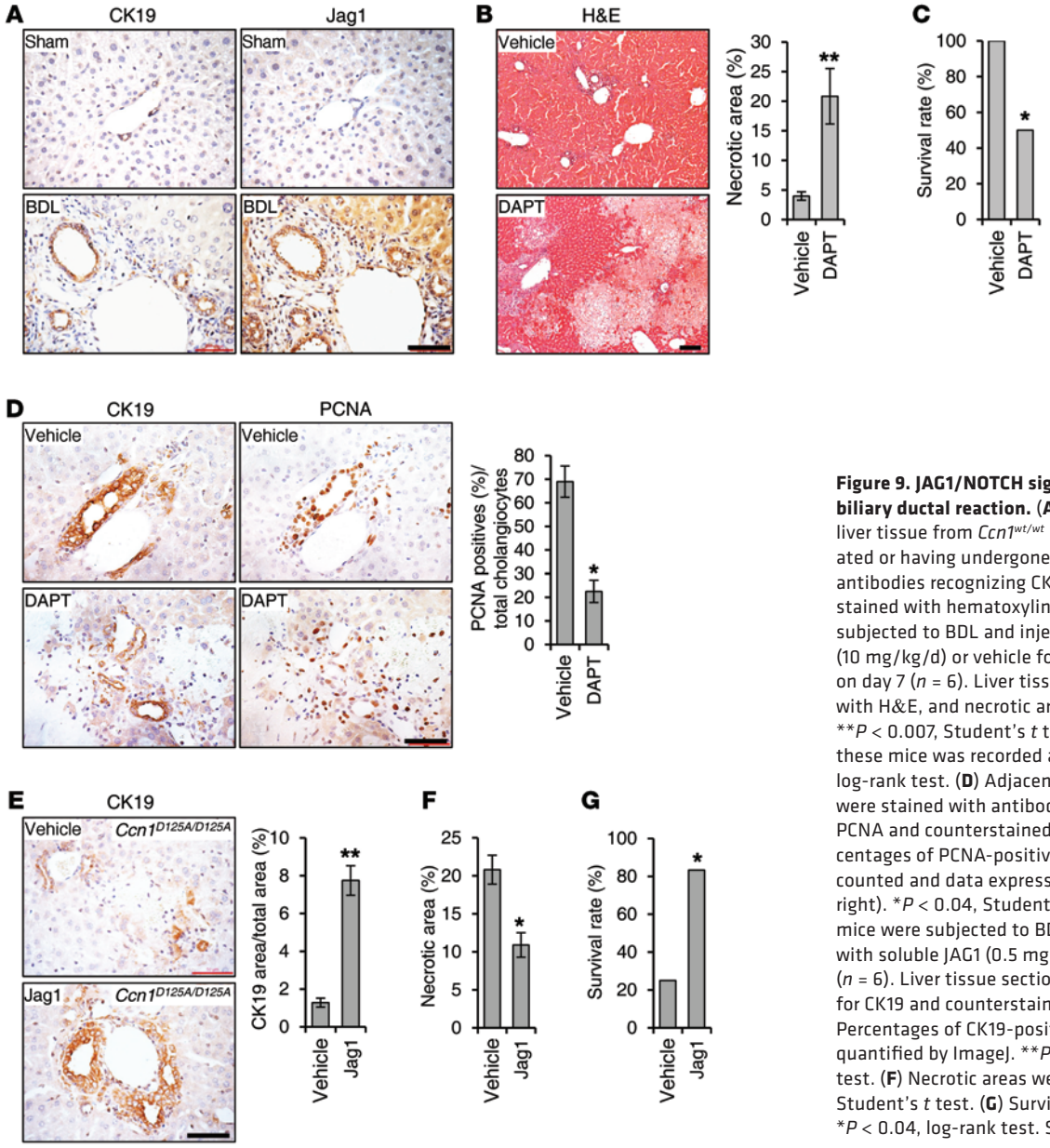

Figure 9. JAG1/NOTCH signaling is critical for biliary ductal reaction. (**A**) Adjacent sections of liver tissue from *Ccn1*$^{wt/wt}$ mice either sham operated or having undergone BDL were stained with antibodies recognizing CK19 or JAG1 and counterstained with hematoxylin. (**B**) *Ccn1*$^{wt/wt}$ mice were subjected to BDL and injected i.p. daily with DAPT (10 mg/kg/d) or vehicle for 6 days and sacrificed on day 7 (n = 6). Liver tissue sections were stained with H&E, and necrotic areas were quantified. $^{**}P < 0.007$, Student's t test. (**C**) Survival rate of these mice was recorded after 7 days. $^{*}P < 0.04$, log-rank test. (**D**) Adjacent sections of liver tissue were stained with antibodies recognizing CK19 or PCNA and counterstained with hematoxylin. Percentages of PCNA-positive cholangiocytes were counted and data expressed as mean ± SD (n = 6, right). $^{*}P < 0.04$, Student's t test. (**E**) *Ccn1*$^{D125A/D125A}$ mice were subjected to BDL, and injected i.p. daily with soluble JAG1 (0.5 mg/kg) or vehicle for 6 days (n = 6). Liver tissue sections were immunostained for CK19 and counterstained with hematoxylin. Percentages of CK19-positive tissue areas were quantified by ImageJ. $^{**}P < 0.007$, Student's t test. (**F**) Necrotic areas were quantified. $^{*}P < 0.04$, Student's t test. (**G**) Survival rate was recorded. $^{*}P < 0.04$, log-rank test. Scale bars: 50 μm.

tured WT HPCs with HSCs from *Ccn1*$^{wt/wt}$ or *Ccn1*$^{D125A/D125A}$ mice. Coculture of HPCs with HSCs from *Ccn1*$^{wt/wt}$ mice led to increased expression of NOTCH target genes such as *Hes1* and cholangiocyte markers, including *Hnf1b*, *Hnf6*, and *CK19*, whereas expression of hepatocyte markers such as *Hnf1a* and *Hnf4a* was not altered, consistent with cholangiocyte differentiation of HPCs (refs. 49, 50, and Figure 8E). However, when WT HPCs were cocultured with HSCs from *Ccn1*$^{D125A/D125A}$ mice, expression of cholangiocytes markers (*Hes1*, *Hnf1b*, *Hnf6*, and *CK19*) was significantly diminished compared with coculture with WT HSCs, without any effect on hepatocyte marker expression (Figure 8E), indicating that *Ccn1*$^{D125A/D125A}$ HSCs are impaired in their ability to promote HPCs' differentiation into cholangiocytes. Thus, CCN1 promotes cholangiocyte differentiation from progenitor cells through induction of *Jag1* in hepatic fibroblasts. This conclusion is supported by double immunofluorescence staining of liver sections of mice after 6 weeks of DDC diet, revealing expression of JAG1 in α-smooth muscle actin–positive hepatic fibroblasts in WT mice, but JAG1 expression was greatly impaired in hepatic fibroblasts of *Ccn1*$^{D125A/D125A}$ mice (Figure 8F).

NF-κB and Notch signaling are required for cholangiocyte proliferation and ductular reaction in vivo. To assess the significance of CCN1-induced NF-κB activation of JAG1/NOTCH signaling in ductular reaction in vivo, we first examined JAG1 protein staining by immunohistochemistry. Like CCN1, JAG1 was detected at a low level in normal liver but was elevated in cholangiocytes after BDL treatment in WT mice, suggesting a role in ductular response (Figure 9A). Remarkably, when *Ccn1*$^{wt/wt}$ mice were subjected to BDL and injected i.p. daily with DAPT for 6 days to block NOTCH signaling, these mice suffered massive hepatic necrosis with approximately 20% necrotic area in the liver parenchyma and significantly reduced survival in a 7-day period, resembling the response of

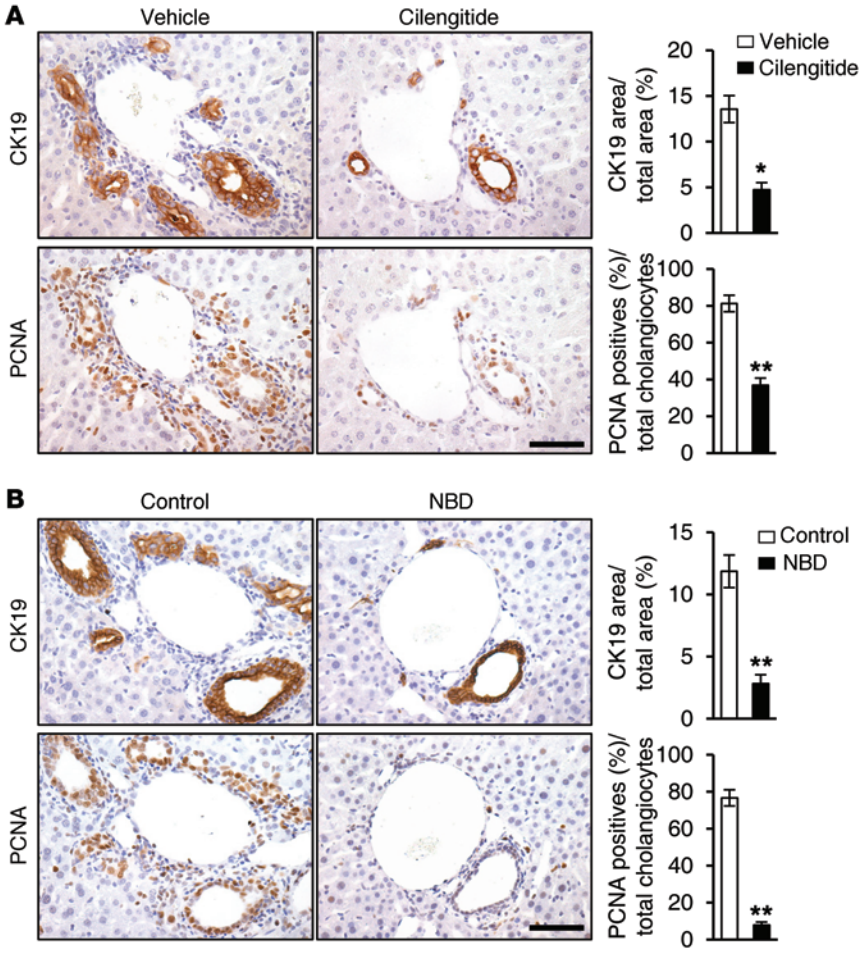

Figure 10. Blockade of integrins $\alpha_v\beta_3$ and $\alpha_v\beta_5$ and NF-κB abrogates ductular reaction. (**A**) WT mice were subjected to BDL and treated with either vehicle or cilengitide (10 mg/kg) daily for 6 days; adjacent liver sections were immunostained for CK19 or PCNA. Data were quantified and expressed as mean ± SD. (n = 6 per group.) $^*P < 0.02$, $^{**}P < 0.004$, Student's t test. (**B**) WT mice were subjected to BDL and injected with either NBD or control peptide (1 mg/kg each) daily for 6 days; adjacent liver sections were immunostained for CK19 or PCNA. Data were quantified and expressed as mean ± SD. (n = 6 per group.) $^{**}P < 0.004$, Student's t test. Scale bars: 50 μm.

Ccn1$^{D125A/D125A}$ mice to BDL (Figure 9, B and C, and Figure 2, B and C). DAPT-treated mice suffered impaired ductular reaction and greatly reduced cholangiocyte proliferation after BDL as judged by PCNA staining, and the number of CK19-positive intrahepatic bile ducts around the portal areas was greatly diminished (Figure 9D).

These results confirm that NOTCH signaling is required for cholangiocyte proliferation in ductular reaction, and suggest that deficiencies in CCN1-regulated JAG1/NOTCH signaling underlie the defects in *Ccn1*$^{D125A/D125A}$ mice. This interpretation predicts that treatment of *Ccn1*$^{D125A/D125A}$ mice with soluble JAG1 may rescue their defects in ductular reaction by activating NOTCH signaling. In strong support of this interpretation, daily administration of soluble JAG1 in *Ccn1*$^{D125A/D125A}$ mice after BDL was sufficient to restore cholangiocyte proliferation and bile duct expansion (Figure 9E), leading to reduced hepatic necrosis and enhanced animal survival (Figure 9, F and G). As expected, i.p. injected soluble JAG1 is rapidly and extensively localized in the liver (Supplemental Figure 3).

Since we have shown that CCN1 induces cholangiocyte proliferation through NF-κB activation mediated by integrins $\alpha_v\beta_3$ and $\alpha_v\beta_5$, we investigated their role in ductular reaction. To assess the role of integrins $\alpha_v\beta_3$ and $\alpha_v\beta_5$, WT mice were subjected to BDL and treated with either vehicle or cilengitide to block these integrins. Mice treated with vehicle showed normal ductular reaction as expected, with bile duct expansion and proliferation of CK19-positive cholangiocytes that were positive for PCNA (Figure 10A). Remarkably, mice treated with cilengitide suffered impaired ductular reaction with greatly diminished CK19-positive area and reduced PCNA-positive proliferating cholangiocytes (Figure 10A), indicating that engagement of integrins $\alpha_v\beta_3$ and $\alpha_v\beta_5$ is critical for ductular reaction. Finally, to establish the functional role of NF-κB in ductular reaction in vivo, WT mice subjected to BDL were treated with i.p. injections of either control peptide or the NBD peptide to block NF-κB activation. Strikingly, mice treated with NBD peptide exhibited significantly fewer bile ducts, reduced CK19-positive cholangiocytes, and curtailed cholangiocyte proliferation as judged by PCNA staining, similar to inhibition with cilengitide (Figure 10B). Together, these results show clearly that ductular reaction after BDL is dependent on engagement of $\alpha_v\beta_3$/$\alpha_v\beta_5$ and activation of NF-κB.

Discussion

Regeneration of bile ducts is an injury repair response to biliary damage and includes cholangiocyte proliferation, ductular reaction, and associated inflammation. Fibrogenesis may ensue if the injury is chronic and elicits persistent inflammation. Although prominent in cholestatic diseases, ductular reaction is also observed in many acute and chronic liver diseases and is emerging as a driver of progenitor cell contribution to parenchymal regeneration, fibrogenesis, and hepatobiliary neoplasia (3, 16). Dynamic changes in the ECM are thought to be a critical compo-

nent of ductular reaction (16); however, the molecular mechanism of how matrix signaling participates in this context is not well understood. Here we uncover the matricellular protein CCN1 as a novel and critical mediator of ductular reaction and biliary repair. Acting through integrin $\alpha_v\beta_5/\alpha_v\beta_3$–dependent activation of NF-κB and JAG1/NOTCH signaling, CCN1 regulates cholangiocyte proliferation and differentiation from HPCs to participate in ductular reaction. These findings implicate the activation of NF-κB in sterile inflammation as an important mechanism for triggering ductular reaction, and indicate that activation of the CCN1/$\alpha_v\beta_5$/NF-κB/JAG1 axis may promote repair in cholestatic injuries.

Despite extensive knowledge on the role of NF-κB in hepatic inflammation and hepatocellular carcinoma (51), relatively little is known about NF-κB functions in cholangiocytes and biliary injury repair. It was found that inhibition of NF-κB increased hepatocyte apoptosis after BDL (52), and genetic ablation of both IKK1 and IKK2, IκB kinases important for NF-κB activation, leads to inflammatory damage to portal bile ducts (53). However, the role of NF-κB in cholangiocyte proliferation and ductular reaction has not been defined. Here we show that CCN1 acts through integrin-mediated activation of NF-κB to induce ductular reaction, which subsumes an inflammatory response. Indeed, the production of inflammatory cytokines is a feature of "reactive cholangiocytes" found at the ductular reaction niche, whereas resting cholangiocytes do not express these molecules (1). Since NF-κB is a master transcription factor that regulates many genes including those that promote inflammation, cell proliferation, and cell survival (54), it is likely that CCN1 may also induce multiple aspects of reactive cholangiocytes through the activation of NF-κB, including the expression of inflammatory cytokines (Supplemental Figure 7).

Aside from its essential roles in cardiovascular development (20, 21), CCN1 is emerging as a critical regulator of inflammation and injury repair (17, 23, 24, 55). CCN1 is composed of 4 structural domains encoded by discrete, conserved exons that bind different integrin receptors and thereby exert distinct biological effects on various cell types (17, 19). Although CCN1 is accumulated to a high level in hepatocytes in response to BDL (Figure 1A), deletion of *Ccn1* in hepatocytes in $Ccn1^{\Delta Hep}$ mice had no effect on cholangiocyte proliferation and ductular reaction (Figures 2 and 3). Germline knock-in mutations that disrupt CCN1 binding to integrin $\alpha_6\beta_1$ also had no effect, whereas a single amino acid substitution (D125A) mutation abolishing CCN1 binding to $\alpha_v\beta_5/\alpha_v\beta_3$ severely diminished ductular reaction in vivo (Figures 2 and 3). Mechanistically, CCN1 activates NF-κB and *Jag1* expression to induce cholangiocyte proliferation through integrin $\alpha_v\beta_5$ with $\alpha_v\beta_3$ playing an auxiliary role (Figures 4 and 5). Furthermore, blockade of $\alpha_v\beta_5/\alpha_v\beta_3$ by cilengitide severely impaired ductular reaction after BDL (Figure 10A). Although several integrins, particularly $\alpha_v\beta_6$, have been previously associated with cholangiocyte functions (42), the role of $\alpha_v\beta_5/\alpha_v\beta_3$ in cholangiocytes and ductular reaction was previously unknown.

The essential role of the JAG1 and NOTCH2 receptor-ligand pair in bile duct formation during embryonic development has been well established. Mutations in *JAG1* or *NOTCH2* result in Alagille syndrome, phenotypes of which include intrahepatic bile duct paucity and in some cases biliary atresia (8–10). Recent studies have implicated NOTCH signaling in liver repair, and *Jag1* expression from hepatic fibroblasts was shown to promote cholangiocyte differentiation from HPCs and contribute to repair (14, 56). However, the critical role of JAG1/NOTCH signaling in the proliferation of differentiated cholangiocytes was not previously defined (7, 15). Since $Ccn1^{D125A/D125A}$ mice do not show any developmental defect in the biliary system, it is likely that *Jag1* is regulated by CCN1 only in response to hepatic injury and not during ontogeny. Furthermore, NOTCH1 appears to be the principal partner of JAG1 in LMCCs (Figure 6A), suggesting the possibility that NOTCH1 and NOTCH2 may have distinct functions in cholangiocyte differentiation and proliferation (12, 13). Nonetheless, NOTCH2 may also play a role in injury repair, since *Notch2*-deficient mice show defects in tubular morphogenesis after DDC diet (56).

CCN1 induces *Jag1* expression in bile duct cholangiocytes through NF-κB activation to promote proliferation (Figures 5–7). In addition, CCN1 also induces *Jag1* expression in activated HSCs, which acts in juxtacrine to stimulate the differentiation of HPCs into cholangiocytes (Figure 8 and ref. 14). A role for CCN1 in HPC differentiation into cholangiocytes explains the impaired ductular reaction observed after chronic DDC diet, in which participation of HPCs is thought to play a major role (37). However, lineage tracing studies may be required to determine the precise cellular origins of reactive cholangiocytes in response to BDL or DDC diet (16).

Consistent with CCN1 induction of cholangiocyte proliferation and ductular reaction through the $\alpha_v\beta_5$/NF-κB/JAG1 axis, inhibitors of $\alpha_v\beta_5/\alpha_v\beta_3$ engagement (cilengitide), NF-κB activation (NBD peptide), and NOTCH signaling (DAPT) each severely impaired ductular reaction in WT mice after BDL, whereas soluble JAG1 stimulated ductular reaction (Figures 9 and 10). Although NOTCH receptors and NOTCH ligands are usually expressed as transmembrane proteins in different cell types that interact in juxtacrine, soluble JAG1 extracellular domain released through proteolytic cleavage has been identified in several biological systems, suggesting biological functions of soluble JAG1 through paracrine action (46, 57–59). Systemic injection of soluble JAG1 peptide has been shown to activate NOTCH signaling in vivo (60, 61). We show herein that soluble JAG1 activates NOTCH signaling in vitro by inducing NICD release and promoting cholangiocyte proliferation (Figure 6, C, E, and I). Remarkably, administration of soluble JAG1 efficiently induced cholangiocyte proliferation (Figure 7) and restored ductular reaction and enhanced survival in $Ccn1^{D125A/D125A}$ mice (Figure 9, E–G), strongly supporting the notion that deficits in CCN1-regulated *Jag1* expression underlie the ductular reaction defects in $Ccn1^{D125A/D125A}$ mice.

In addition to impaired ductular reaction, $Ccn1^{D125A/D125A}$ mice also suffered massive hepatic necrosis after BDL, although there was no difference from WT mice in bile acid production or hepatocyte sensitivity to bile acid (Figure 2 and Supplemental Figure 1). Since bile duct expansion may serve to contain the accumulating bile acid from BDL, we interpret the massive hepatic necrosis in $Ccn1^{D125A/D125A}$ mice to be a secondary effect of impaired ductular reaction, resulting in insufficient bile ducts to shield bile acid from the parenchyma. This interpretation is supported by the observation that inhibiting (Figure 9, B–D) or restoring (Figure 9, E–G) cholangiocyte proliferation and ductular reaction using approaches independent of *Ccn1* mutation leads to enhanced or reduced hepatic necrosis, respectively.

Ccn1 is a growth factor–inducible immediate-early gene that is transcriptionally activated by a variety of stimuli (62). As a known target gene of the YAP transcriptional coactivator (63, 64), *Ccn1* may mediate some of the effects of the Hippo pathway. Recent studies have shown that deletion of YAP in the liver compromises ductular reaction after BDL with increased parenchymal necrosis (65), suggesting that impaired *Ccn1* expression might have contributed to the observed phenotypes.

Ductular reaction has been suggested to serve as the "pacemaker of portal fibrosis," since activated cholangiocytes are a source of growth factors and cytokines that recruit and activate HSCs and portal fibroblasts, which are major precursors of ECM-producing myofibroblasts contributing to liver fibrosis (66). Recent studies showed that CCN1 is induced in liver injuries and functions to dampen and resolve liver fibrosis by inducing cellular senescence in activated myofibroblasts, triggering the ECM-producing myofibroblasts to express an antifibrotic phenotype characteristic of senescence (24, 67). Since CCN1 can function to limit and resolve liver fibrosis, it appears paradoxical that CCN1 also orchestrates ductular reaction, which can promote a fibrotic response if it becomes chronic. However, the antifibrotic effects of CCN1 are mediated through binding to integrin $\alpha_6\beta_1$ in its carboxy terminal domain (23, 24), whereas the induction of ductular reaction is mediated through binding of CCN1 to integrins $\alpha_v\beta_5/\alpha_v\beta_3$ through the von Willebrand type C repeat located in the N-terminal half of CCN1 (17). It appears likely that CCN1 may regulate different aspects of injury repair via disparate activities mediated through its distinct structural domains, which appear to have emerged from exon shuffling in evolution to combine different activities relevant to wound healing.

Although cholangiocyte proliferation is a prominent initial response in cholestasis, ductopenia is a common feature of advanced cholangiopathies, and thus understanding how cholangiocyte proliferation and bile duct regeneration are regulated may provide opportunities for the management of ductopenic pathologies (7). Results presented herein reveal previously unknown roles of the CCN1/$\alpha_v\beta_5$/NF-κB/JAG1 axis in cholangiocyte proliferation and ductular reaction. These new insights into cholangiocyte proliferation and bile duct regeneration pathways may be exploited in future studies exploring potential therapeutic strategies in treating cholestatic diseases.

Methods

Animals and liver cholestasis induction. *Alb-Cre Ccn1*$^{fl/fl}$ (*Ccn1*$^{\Delta Hep}$) mice (24) and *Ccn1*$^{dm/dm}$ mice (27) were constructed as described previously. *Ccn1*$^{D125A/D125A}$ knock-in mice were made in a similar way by replacement of the *Ccn1* genomic locus with the *Ccn1-D125A* allele encoding a CCN1 mutant with Asp to Ala substitution at amino acid 125, disrupting CCN1 binding to integrins $\alpha_v\beta_5$ and $\alpha_v\beta_3$ (32). The construction of *Ccn1*$^{D125A/D125A}$ knockin mice uses the same procedure and strategy as the construction of *Ccn1*$^{dm/dm}$ knockin mice (27). All *Ccn1*$^{\Delta Hep}$, *Ccn1*$^{dm/dm}$, and *Ccn1*$^{D125A/D125A}$ mice were generated in svJ129-C57BL/6 mixed background and backcrossed into C57BL/6 background more than 6, more than 20, and more than 4 times, respectively. All mice used were 2- to 3-month-old males kept in the University of Illinois barrier facility (accredited by the Association for Assessment and Accreditation of Laboratory Animal Care International) with veterinary care.

BDL was performed as described previously (33), and sham operations were performed as controls. To examine the role of JAG1/NOTCH signaling, where indicated, soluble rat JAG1-Fc (500 μg/kg; R&D Systems) or vehicle was injected i.p. after BDL, or DAPT (*N*-[*N*-(3,5-difluorophenacetyl)-L-alanyl]-S-phenylglycine *t*-butyl ester; Sigma-Aldrich) solubilized in corn oil was injected i.p. (10 mg/kg) for 6 days and mice euthanized on the seventh day. Where indicated, NBD peptide (DRQIKIWFQNRRMKWKK-TALDWSWLQTE) or control peptide (DRQIKIWFQNRRMKWKK, 1 mg/kg) obtained from Novus Biologicals was injected at 1 mg/kg after BDL. For DDC (3,5-diethoxycarbonyl-1,4-dihydrocollidine; Sigma-Aldrich) diet, mice from each genotype were fed either a standard control diet or the control diet supplemented with 0.1% DDC, and liver tissues collected after 6 weeks (68).

To examine the mitogenic effects of CCN1 or soluble JAG1 on cholangiocyte proliferation in normal mouse liver, proteins (CCN1, 1 mg/kg; JAG1, 0.5 mg/kg) were injected daily via retro-orbital delivery (69) for 2–4 days. Likewise, DAPT (10 mg/kg), BAY11-7082 (5 mg/kg; Sigma-Aldrich), cilengitide (10 mg/kg; Selleckchem), and NBD peptide or control peptide were coinjected where indicated.

Cell preparation and culture. Freshly isolated primary cholangiocytes were purified by immunoaffinity separation with an mAb, rat IgG2a (provided by R. Faris, Brown University, Providence, Rhode Island, USA), against an antigen expressed by mouse cholangiocytes as described previously (70). Cells in the preparation were 98.5% ± 0.4% positive for the IgG2a antigen as assessed by immunocytochemistry. HSCs were isolated from a nonparenchymal cell fraction as described previously (71). Mouse HPCs were isolated as described previously (72). In brief, HPCs were purified by centrifugation through a discontinuous gradient of 20% and 50% Percoll in PBS at 1,400 *g* for 20 minutes. The lower of 2 thin bands in the 20% Percoll fraction was collected and confirmed by immunostaining with anti-DLK1 antibody (ab21682; Abcam). Coculture of HPCs with HSCs was carried out as described previously (14). Immortalized large murine cholangiocyte lines (LMCC) were maintained as described previously (73). WT CCN1, mutant proteins (D125A and DM), soluble JAG1, DAPT, BAY11-7082, NBD peptide, or NBD control peptide were added to culture medium as indicated.

Serum biochemistry analysis. The serum levels of alanine aminotransferase, aspartate aminotransferase, and alkaline phosphatase were analyzed by the Biologic Resources facility at the University of Illinois at Chicago.

Histology, immunohistochemistry, and human liver tissue array. Tissues were formalin-fixed and paraffin-embedded and 6-μm sections prepared. To quantify parenchymal necrosis, photomicrographs of 6 randomly selected areas (3.4 × 2.5 mm^2) were taken from each animal using a Leica DM4000B microscope mounted with QI Click CCD digital camera (QImaging) and images analyzed using NIH ImageJ software. The percentage of necrosis was evaluated by measurement of necrotic areas/total area of tissue minus the area of the vascular lumen. For immunohistochemistry, epitopes were unmasked by incubation with sodium citrate, pH 6.0, and incubated with primary antibodies against CCN1 (24), CK19 (10712-1-AP; Proteintech), PCNA (ab29; Abcam), and JAG1 (ab7771; Abcam) overnight. Secondary antibody (GE Healthcare) was conjugated with HRP, and 3,3′-diaminobenzidine (Sigma-Aldrich) was used as chromogen. Samples were counterstained with hematoxylin. Liver tissue array (US Biomax Inc.) was

used in order to detect CCN1 in human liver. Twelve photomicrographs of CK19-positive areas (×10 magnification) were taken from each section for every animal; and the ratio of the CK19-positive area to total area was calculated using NIH ImageJ software.

BrdU incorporation. For BrdU incorporation, cholangiocytes were incubated with BrdU (10 μg/ml; Roche Applied Science) for 25 or 45 minutes, then fixed, washed, and probed with FITC-conjugated anti-BrdU antibodies (MAB3262F; Millipore). BrdU-positive cells from fluorescence images taken from 5 random high-power fields were scored and normalized against DAPI-positive cells. All assays were done in triplicate, and approximately 300 cells were counted in each sample.

Western blots. Western blot analyses were performed using standard procedure with enhanced chemiluminescence using an ECL system (GE Healthcare). Antibodies against the following proteins were used: sheep anti–mouse CCN1 (AF4055; R&D Systems), rabbit anti-JAG1 (ab7771; Abcam), rabbit anti-NOTCH1 (sc6014; Santa Cruz Biotechnology), rabbit anti-NOTCH2 (sc5545; Santa Cruz Biotechnology), rabbit anti–phospho-p65 (3033; Cell Signaling), rabbit anti-p65 (3034; Cell Signaling), and anti–β-actin (mAbcam8226; Abcam).

RNA isolation and quantitative RT-PCR. Total RNA was purified from liver tissue and cultured cells using RNeasy Mini Kit (Qiagen) following manufacturer's protocol. RNA was reverse transcribed using Superscript Reverse Transcriptase III (Invitrogen). Quantitative RT-PCR (qRT-PCR) was performed by mixing of cDNA and gene-specific primers (Supplemental Table 1) with iQ SYBR Green Supermix (Bio-Rad), and reactions carried out in iCycler Thermal Cycler (Bio-Rad). PCR specificity was confirmed by agarose gel electrophoresis and melting curve analysis. A housekeeping gene (*cyclophilin E*) was used as an internal standard.

RNA interference. Cells were transfected with 10 nM siRNA targeting *Ccn1*, *Itgav*, *Itga6*, *Itgb3*, *Itgb5*, *Itgb6*, *Jag1*, *Notch1*, *p65*, or a nontargeting sequence control siRNA (Integrated DNA Technologies) using Lipofectamine RNAiMAX reagent (Invitrogen) according to manufacturer's protocol. Gene expression was analyzed by RT-PCR 48 hours after transfection. Sequences used for siRNA knockdown are shown in Supplemental Table 2.

Adenoviral infection. HSC or cholangiocytes were infected with adenovirus expressing β-galactosidase (*LacZ*) or *Ccn1* for 48 hours at a multiplicity of infection of approximately 500 PFU per cell.

Statistics. Data are expressed as mean ± SD. All experiments were repeated at least 3 times with similar results. The 2-tailed Student's *t* test was performed to determine the probability of statistically significant difference (*P* values) and recorded in figure legends. Survival curves were calculated using the Kaplan-Meier method. Statistical significance for survival between populations was analyzed by log-rank test. A *P* value less than 0.05 was considered statistically significant.

Study approval. All animal experiments followed procedures approved by the IACUC of the University of Illinois at Chicago.

Supplemental Methods. For all methods not listed here, please refer to the online Supplemental Methods section.

Acknowledgments

We thank Seung Won Shin and Guoqiang Yan for excellent assistance, and members of the laboratory for helpful discussion. This work was supported by a grant from the NIH (R01-GM78492) to L.F. Lau, and in part by the Dr. Nicholas C. Hightower Centennial Chair of Gastroenterology from Scott & White and a VA Merit Award to G. Alpini. The views expressed herein are those of the authors and do not necessarily reflect the views of the NIH or the Department of Veterans Affairs.

Address correspondence to: Lester F. Lau, Department of Biochemistry and Molecular Genetics, University of Illinois at Chicago College of Medicine, 900 South Ashland Avenue, Chicago, Illinois 60607, USA. Phone: 312.996.6978; E-mail: LFLau@uic.edu.

1. Lazaridis KN, Strazzabosco M, LaRusso NF. The cholangiopathies: disorders of biliary epithelia. *Gastroenterology*. 2004;127(5):1565–1577.
2. Tabibian JH, Masyuk AI, Masyuk TV, O'Hara SP, LaRusso NF. Physiology of cholangiocytes. *Compr Physiol*. 2013;3(1):541–565.
3. Gouw AS, Clouston AD, Theise ND. Ductular reactions in human liver: diversity at the interface. *Hepatology*. 2011;54(5):1853–1863.
4. Roskams TA, et al. Nomenclature of the finer branches of the biliary tree: canals, ductules, and ductular reactions in human livers. *Hepatology*. 2004;39(6):1739–1745.
5. Park SM. The crucial role of cholangiocytes in cholangiopathies. *Gut Liver*. 2012;6(3):295–304.
6. Glaser SS, et al. Recent advances in the regulation of cholangiocyte proliferation and function during extrahepatic cholestasis. *Dig Liver Dis*. 2010;42(4):245–252.
7. Franchitto A, et al. Recent advances on the mechanisms regulating cholangiocyte proliferation and the significance of the neuroendocrine regulation of cholangiocyte pathophysiology. *Ann Transl Med*. 2012;1(3):27.
8. Li L, et al. Alagille syndrome is caused by mutations in human Jagged1, which encodes a ligand for Notch1. *Nat Genet*. 1997;16(3):243–251.
9. Oda T, et al. Mutations in the human Jagged1 gene are responsible for Alagille syndrome. *Nat Genet*. 1997;16(3):235–242.
10. McDaniell R, et al. NOTCH2 mutations cause Alagille syndrome, a heterogeneous disorder of the notch signaling pathway. *Am J Hum Genet*. 2006;79(1):169–173.
11. Lozier J, McCright B, Gridley T. Notch signaling regulates bile duct morphogenesis in mice. *PLoS One*. 2008;3(3):e1851.
12. McCright B, Lozier J, Gridley T. A mouse model of Alagille syndrome: Notch2 as a genetic modifier of Jag1 haploinsufficiency. *Development*. 2002;129(4):1075–1082.
13. Geisler F, et al. Liver-specific inactivation of Notch2, but not Notch1, compromises intrahepatic bile duct development in mice. *Hepatology*. 2008;48(2):607–616.
14. Boulter L, et al. Macrophage-derived Wnt opposes Notch signaling to specify hepatic progenitor cell fate in chronic liver disease. *Nat Med*. 2012;18(4):572–579.
15. Geisler F, Strazzabosco M. Emerging roles of Notch signaling in liver disease. *Hepatology*. 2015;61(1):382–392.
16. Williams MJ, Clouston AD, Forbes SJ. Links between hepatic fibrosis, ductular reaction, and progenitor cell expansion. *Gastroenterology*. 2014;146(2):349–356.
17. Jun JI, Lau LF. Taking aim at the extracellular matrix: CCN proteins as emerging therapeutic targets. *Nat Rev Drug Discov*. 2011;10(12):945–963.
18. Murphy-Ullrich JE, Sage EH. Revisiting the matricellular concept. *Matrix Biol*. 2014;37:1–14.
19. Lau LF. CCN1/CYR61: the very model of a modern matricellular protein. *Cell Mol Life Sci*. 2011;68(19):3149–3163.
20. Mo FE, Muntean AG, Chen CC, Stolz DB, Watkins SC, Lau LF. CYR61 (CCN1) is essential for placental development and vascular integrity. *Mol Cell Biol*. 2002;22(24):8709–8720.
21. Mo F-E, Lau LF. The matricellular protein CCN1 is essential for cardiac development. *Circ Res*. 2006;99(9):961–969.
22. Bai T, Chen C-C, Lau LF. The matricellular protein CCN1 activates a pro-inflammatory genetic program in murine macrophages. *J Immunol*. 2010;184(6):3223–3232.
23. Jun JI, Lau LF. The matricellular protein CCN1 induces fibroblast senescence and restricts fibrosis in cutaneous wound healing. *Nat Cell Biol*. 2010;12(7):676–685.
24. Kim KH, Chen CC, Monzon RI, Lau LF. Matricellular protein CCN1 promotes regression of

liver fibrosis through induction of cellular senescence in hepatic myofibroblasts. *Mol Cell Biol*. 2013;33(10):2078–2090.
25. Hu M, et al. Wnt/β-catenin signaling in murine hepatic transit amplifying progenitor cells. *Gastroenterology*. 2007;133(5):1579–1591.
26. Alpini G, Lenzi R, Sarkozi L, Tavoloni N. Biliary physiology in rats with bile ductular cell hyperplasia. Evidence for a secretory function of proliferated bile ductules. *J Clin Invest*. 1988;81(2):569–578.
27. Chen C-C, Young JL, Monzon RI, Chen N, Todorovic V, Lau LF. Cytotoxicity of TNFα is regulated by integrin-mediated matrix signaling. *EMBO J*. 2007;26(5):1257–1267.
28. Jun JI, Lau LF. Cellular senescence controls fibrosis in wound healing. *Aging (Albany NY)*. 2010;2(9):627–631.
29. Leu S-J, Lam SCT, Lau LF. Proangiogenic activities of CYR61 (CCN1) mediated through integrins αvβ3 and α6β1 in human umbilical vein endothelial cells. *J Biol Chem*. 2002;277(48):46248–46255.
30. Monnier Y, et al. CYR61 and αvβ5 integrin cooperate to promote invasion and metastasis of tumors growing in preirradiated stroma. *Cancer Res*. 2008;68(18):7323–7331.
31. Leu S-J, et al. Targeted mutagenesis of the matricellular protein CCN1 (CYR61): selective inactivation of integrin α6β1-heparan sulfate proteoglycan coreceptor-mediated cellular activities. *J Biol Chem*. 2004;279(42):44177–44187.
32. Chen N, Leu S-J, Todorovic V, Lam SCT, Lau LF. Identification of a novel integrin αvβ3 binding site in CCN1 (CYR61) critical for pro-angiogenic activities in vascular endothelial cells. *J Biol Chem*. 2004;279(42):44166–44176.
33. Kountouras J, Billing BH, Scheuer PJ. Prolonged bile duct obstruction: a new experimental model for cirrhosis in the rat. *Br J Exp Pathol*. 1984;65(3):305–311.
34. Woolbright BL, Jaeschke H. Novel insight into mechanisms of cholestatic liver injury. *World J Gastroenterol*. 2012;18(36):4985–4993.
35. Faubion WA, et al. Toxic bile salts induce rodent hepatocyte apoptosis via direct activation of Fas. *J Clin Invest*. 1999;103(1):137–145.
36. Fickert P, et al. A new xenobiotic-induced mouse model of sclerosing cholangitis and biliary fibrosis. *Am J Pathol*. 2007;171(2):525–536.
37. Turner R, et al. Human hepatic stem cell and maturational liver lineage biology. *Hepatology*. 2011;53(3):1035–1045.
38. Nakanuma Y. Tutorial review for understanding of cholangiopathy. *Int J Hepatol*. 2012;2012:547840.
39. Alpini G, et al. Morphological, molecular, and functional heterogeneity of cholangiocytes from normal rat liver. *Gastroenterology*. 1996;110(5):1636–1643.
40. Alpini G, et al. Heterogeneity of the proliferative capacity of rat cholangiocytes after bile duct ligation. *Am J Physiol*. 1998;274(4):G767–G775.
41. Meng F, et al. Role of stem cell factor and granulocyte colony-stimulating factor in remodeling during liver regeneration. *Hepatology*. 2012;55(1):209–221.
42. Wang B, et al. Role of alphavbeta6 integrin in acute biliary fibrosis. *Hepatology*. 2007;46(5):1404–1412.
43. Bray SJ. Notch signalling: a simple pathway becomes complex. *Nat Rev Mol Cell Biol*. 2006;7(9):678–689.
44. Bash J, et al. Rel/NF-κB can trigger the Notch signaling pathway by inducing the expression of Jagged1, a ligand for Notch receptors. *EMBO J*. 1999;18(10):2803–2811.
45. Tilstra JS, et al. NF-κB inhibition delays DNA damage-induced senescence and aging in mice. *J Clin Invest*. 2012;122(7):2601–2612.
46. Lu J, et al. Endothelial cells promote the colorectal cancer stem cell phenotype through a soluble form of Jagged-1. *Cancer Cell*. 2013;23(2):171–185.
47. Reardon DA, Cheresh D. Cilengitide: a prototypic integrin inhibitor for the treatment of glioblastoma and other malignancies. *Genes Cancer*. 2011;2(12):1159–1165.
48. Friedman SL. Hepatic stellate cells: protean, multifunctional, and enigmatic cells of the liver. *Physiol Rev*. 2008;88(1):125–172.
49. Shin S, et al. Foxl1-Cre-marked adult hepatic progenitors have clonogenic and bilineage differentiation potential. *Genes Dev*. 2011;25(11):1185–1192.
50. Tanimizu N, Miyajima A, Mostov KE. Liver progenitor cells develop cholangiocyte-type epithelial polarity in three-dimensional culture. *Mol Biol Cell*. 2007;18(4):1472–1479.
51. Luedde T, Schwabe RF. NF-κB in the liver — linking injury, fibrosis and hepatocellular carcinoma. *Nat Rev Gastroenterol Hepatol*. 2011;8(2):108–118.
52. Miyoshi H, Rust C, Guicciardi ME, Gores GJ. NF-κB is activated in cholestasis and functions to reduce liver injury. *Am J Pathol*. 2001;158(3):967–975.
53. Luedde T, Heinrichsdorff J, de Lorenzi R, De Vos R, Roskams T, Pasparakis M. IKK1 and IKK2 cooperate to maintain bile duct integrity in the liver. *Proc Natl Acad Sci U S A*. 2008;105(28):9733–9738.
54. Aggarwal BB. Signalling pathways of the TNF superfamily: a double-edged sword. *Nat Rev Immunol*. 2003;3(9):745–756.
55. Emre Y, Imhof BA. Matricellular protein CCN1/CYR61: a new player in inflammation and leukocyte trafficking. *Semin Immunopathol*. 2014;36(2):253–259.
56. Fiorotto R, et al. Notch signaling regulates tubular morphogenesis during repair from biliary damage in mice. *J Hepatol*. 2013;59(1):124–130.
57. Aho S. Soluble form of Jagged1: unique product of epithelial keratinocytes and a regulator of keratinocyte differentiation. *J Cell Biochem*. 2004;92(6):1271–1281.
58. Campese AF, et al. Mouse Sertoli cells sustain de novo generation of regulatory T cells by triggering the notch pathway through soluble JAGGED1. *Biol Reprod*. 2014;90(3):53.
59. Pelullo M, et al. Notch3/Jagged1 circuitry reinforces notch signaling and sustains T-ALL. *Neoplasia*. 2014;16(12):1007–1017.
60. Hellstrom M, et al. Dll4 signalling through Notch1 regulates formation of tip cells during angiogenesis. *Nature*. 2007;445(7129):776–780.
61. Okamoto M, Takeda K, Lucas JJ, Joetham A, Yasutomo K, Gelfand EW. Low-dose lipopolysaccharide affects lung allergic responses by regulating Jagged1 expression on antigen-pulsed dendritic cells. *Int Arch Allergy Immunol*. 2012;157(1):65–72.
62. O'Brien TP, Yang GP, Sanders L, Lau LF. Expression of cyr61, a growth factor-inducible immediate-early gene. *Mol Cell Biol*. 1990;10(7):3569–3577.
63. Zhang H, Pasolli HA, Fuchs E. Yes-associated protein (YAP) transcriptional coactivator functions in balancing growth and differentiation in skin. *Proc Natl Acad Sci U S A*. 2011;108(6):2270–2275.
64. Pobbati AV, Hong W. Emerging roles of TEAD transcription factors and its coactivators in cancers. *Cancer Biol Ther*. 2013;14(5):390–398.
65. Bai H, et al. Yes-associated protein regulates the hepatic response after bile duct ligation. *Hepatology*. 2012;56(3):1097–1107.
66. Desmet VJ. Ludwig symposium on biliary disorders — part I. Pathogenesis of ductal plate abnormalities. *Mayo Clin Proc*. 1998;73(1):80–89.
67. Borkham-Kamphorst E, et al. The anti-fibrotic effects of CCN1/CYR61 in primary portal myofibroblasts are mediated through induction of reactive oxygen species resulting in cellular senescence, apoptosis and attenuated TGF-β signaling. *Biochim Biophys Acta*. 2014;1843(5):902–914.
68. Jelnes P, et al. Remarkable heterogeneity displayed by oval cells in rat and mouse models of stem cell-mediated liver regeneration. *Hepatology*. 2007;45(6):1462–1470.
69. Yardeni T, Eckhaus M, Morris HD, Huizing M, Hoogstraten-Miller S. Retro-orbital injections in mice. *Lab Anim (NY)*. 2011;40(5):155–160.
70. Glaser SS, et al. Morphological and functional heterogeneity of the mouse intrahepatic biliary epithelium. *Lab Invest*. 2009;89(4):456–469.
71. Weiskirchen R, Gressner AM. Isolation and culture of hepatic stellate cells. *Methods Mol Med*. 2005;117:99–113.
72. Tirnitz-Parker JE, Tonkin JN, Knight B, Olynyk JK, Yeoh GC. Isolation, culture and immortalisation of hepatic oval cells from adult mice fed a choline-deficient, ethionine-supplemented diet. *Int J Biochem Cell Biol*. 2007;39(12):2226–2239.
73. Ueno Y, et al. Evaluation of differential gene expression by microarray analysis in small and large cholangiocytes isolated from normal mice. *Liver Int*. 2003;23(6):449–459.